Isolation and characterization of synaptic structures from human neural organoids

Marie S. Øhlenschlæger[1], Lucrezia Criscuolo[1], Pia Jensen[1], Daniel J. Lloyd-Davies Sánchez[2], Magdalena Sutcliffe[2], Santosh Bhosale[1], Helle Bogetofte[1], Muhammad Tahir[1], Lene A. Jakobsen[1], Maria Pihl[3], Jonathan Brewer[1], Veit Schwämmle[1], Frantz R. Poulsen[6], Kristine Freude[3], Madeline A. Lancaster[2], Phillip J. Robinson[5], Martin R. Larsen[1].

[1]Department of biochemistry and molecular biology, University of Southern Denmark, Odense, Denmark
[2]MRC Laboratory of Molecular Biology, Cell Biology Division, Cambridge, United Kingdom
[3]Faculty of Health and Medical Sciences, University of Copenhagen, Copenhagen, Denmark
[4]Faculty of Medicine and Health, University of Sydney, Sydney, Australia
[6]Department of Health, Odense University Hospital, University of Southern Denmark, Odense, Denmark

Keywords: Brain organoid, neural organoid, air-liquid interface cerebral organoid, guided dorsal forebrain organoid, synapse, synaptosomes, nerve terminals, growth cone, stimulation, proteomics, phosphorylation, subcellular enrichment

Abstract

Synapses are essential for neuronal function and are central to numerous neurological disorders including developmental and neurodegenerative diseases. Synapses structurally constitute a very small proportion of a neuron, and their protein content is difficult to study using whole tissue preparations. Especially studying synapses on the functional level is challenging. To overcome this limitation, synapses can be captured as synaptosomes generated through enrichment of isolated nerve terminals. Such synaptosomes have a re-sealed plasma membrane and can regenerate their membrane potential and perform physiological function, for example neurotransmitter release.

Synaptosomes are traditionally enriched from rodent or postmortem human brain tissue, but rodent models lack human-specific synaptic features, and the functionality of synaptosomes from postmortem tissues is limited by the postmortem interval and often only show disease endpoints. Furthermore, due to ethical issues and availability, only a few studies have been conducted on human samples. However, neural organoids (NOs) have emerged as a possible new source for isolation of intact and live human nerve terminals to study human-specific aspects of synaptic transmission. Further, the enrichment of synaptosomes is usually performed using density gradient centrifugation, which requires a lot of starting material. In the present study we developed a method for the enrichment of synaptic structures from human NOs applying a differential centrifugation protocol. We then used mass spectrometry-based quantitative proteomics to document the enrichment of synapse and growth cone specific proteins, and quantitative phosphoproteomics upon KCl stimulation to demonstrate viability and physiological function of the derived synaptic structures.

Introduction

Synapses are essential for transmission of signals between neurons. Mutations in synaptic genes have been implicated in over 130 neurological conditions, comprising both neurodevelopmental and neurodegenerative diseases [1] and include autism spectrum disorders (ASD) [2, 3], schizophrenia [4, 5], epilepsy [6], Alzheimer's disease [7, 8] and Parkinson's disease [9, 10]. A commonly used method to study synapses is density-based enrichment of isolated nerve terminals called synaptosomes. Synaptosomes are formed when brain tissue is homogenized in an iso-osmotic buffer, resulting in detachment of the synaptic boutons from the axons followed by resealing of the synaptic membrane (see **fig. 1A**) [11, 12]. Synaptosomes contain mitochondria, synaptic vesicles, and electron dense active zone (AZ) areas with docked vesicles, which can be visualized with transmission electron microscopy (TEM). Frequently, the postsynaptic density (PSD) remains attached to the AZ areas. Synaptosomes are viable and metabolically active when allowed to respire in a suiting buffer [13-15]. Furthermore, synaptosomes can regenerate their membrane potential and be depolarized by chemical stimulation with e.g., a high KCl concentration, leading to neurotransmitter release by synaptic vesicle exocytosis [13, 14, 16].

The traditional methods for enrichment of synaptosomes use different kinds of discontinuous density gradient centrifugation [15, 17-20]. In these protocols the brain tissue is first homogenized in an iso-osmotic sucrose/EDTA buffer followed by an initial low-force centrifugation (800-1,000xg) pelleting nuclei and whole cells in the so-called P1 fraction. The first supernatant (S1) can then be subjected to density gradient centrifugation resulting in subcellular fractionation of the material yielding purified fractions of synaptosomes. If a pure fraction is not required, the density gradient centrifugation can be replaced by a simple second centrifugation step at a higher speed, resulting in a so-called crude synaptosome fraction [21].

Synapses have a complex composition comprising several thousand different proteins involved in processes essential for synaptic function such as synaptic vesicle cycling, neurotransmitter release and synaptic plasticity [22]. Studies of synaptosomes have played important roles in synapse research with significant contributions to the present knowledge about different kinds of neurotransmitters and synaptic protein composition and functions [21] (see **fig. 1B** for example applications). Synaptosome research has furthermore benefitted from the fast development in mass spectrometry (MS)-based proteomic techniques that now enables reliable, large-scale identification and quantification of thousands of proteins in one study [23, 24], together with characterization of various post-translational modifications (PTMs) of proteins, such as phosphorylation, glycosylation, cysteine modifications, acetylation and ubiquitination [25-31]. MS-based proteomic studies of synaptosomes have been utilized in studies of numerous neurological disorders such as Alzheimer's disease [32-37], schizophrenia [38-43] and Parkinson's disease [44-48]. The combination of techniques has furthermore been used to study stimulation-related changes in PTMs of synaptic proteins, mainly phosphorylation, providing a platform to study PTM-regulated signaling in synaptic transmission [31, 49-51]. Studies of depolarization-induced protein phosphorylation in

synaptosomes have shown changes in phosphorylation of proteins that are active in synaptic vesicle cycling including endo- and exocytosis, actin dynamics and AZ proteins involved in neurotransmitter release [49-51]. Previous studies have also indicated a fast and dynamic regulation of sialylation of glycoproteins in isolated nerve terminals, contribution to synaptic transmission [31].

Synaptosome enrichment methods have traditionally been applied to rodent or postmortem human brain tissue. However, the animal models are often not adequate when it comes to clinical translation into humans in e.g., drug development [52], whereas synaptosome functionality of postmortem tissue is limited by the postmortem interval and often only provides information about disease endpoints. Our previous attempts to isolate nerve terminals from *in vitro* 2D cultured human neurons have resulted in very low yield and inconsistent enrichment (data not shown). The relatively recent emergence of the neural organoid (NO) field, where human pluripotent stem cells (PSCs) are differentiated in 3D cell cultures resulting in the development of brain-like tissue, could therefore provide a valuable source of living human synapses that could be enriched more efficiently than from 2D cultures. NOs provide a faithful representation of human brain in vitro: they recapitulate the cellular events in early human brain development [53, 54] and their gene expression has been shown to resemble that of the human fetal brain [54-56]. The 3D culture of NOs promotes increased cellular interaction and cytoarchitectural organization of the neurons into cortical layers in a timed manner reminiscent of the developing brain [53]. This leads to higher complexity and cellular diversity than in 2D cultures. The presence of a range of cell types in NOs (excitatory neurons, inhibitory neurons, intermediate progenitors, radial glia cells and astrocytes [54, 57-59]) allows for development of functional synapses as detected by immunohistochemical (IHC) labeling of synaptic markers and studies of electrical activity [60-65]. Spontaneous electrical activity has been recorded from NOs as early as 52-85 days of differentiation [54, 59] with later development of more coordinated network activity (3-4 months) [65] and complex dendritic morphology (day 80 of differentiation) [54, 66], suggesting progressive maturation of synapse physiology. Using NO tissue for synaptosome preparation could therefore provide a platform for studying synapses developed from patient-derived, induced PSCs (iPSCs), enabling functional studies of synapses in relation to diseases and drug development in a human setting. Additionally, synaptic function and synapse development could be studied in a controllable *in vitro* system that can be manipulated e.g., by CRISPR/Cas9 genetical engineering, labeling, or various kinds of stimulations.

The aim of the present study was to develop a method for the enrichment of viable synaptosomes from human NOs to study molecular mechanisms underlying synaptic transmission in human synapses in health and disease. The presented method is based on differential centrifugation, inspired by the traditional enrichment of the crude synaptosome fraction and other subcellular fractionation protocols using differential centrifugation for proteomic studies of isolated cellular compartments [67-69]. The present method applies four short differential centrifugations of tissue homogenates. We show that this method can be used to enrich synaptic proteins from newborn and adult mouse and human brain tissues, and from NOs using two different types – guided dorsal forebrain organoids (FBOs) [57, 70] and unguided air-liquid interface cerebral organoids (ALI-COs)

[71]. The method is highly reproducible between the different brain tissues and organoid types, and provides a protocol to study synaptic proteins and synapse development in human NOs. We further demonstrate that synaptosomes from adult mouse tissue enriched with the presented method are viable, showing depolarization-dependent changes in protein phosphorylation after stimulation with high KCl. Applying the method to ALI-COs at day 90 and 150 showed enrichment of growth cone particles (GCPs) and immature synaptic structures (synaptosomes) that respond to KCl stimulation, resulting in changes in protein phosphorylation of cytoskeletal and synaptic proteins. Thus, the method provides enrichment of viable synaptic structures that can be used to study synaptic proteins in human NOs during development or in a disease setting.

Methods

Generation of dorsal forebrain organoids

Human iPSCs (IMR90-4 cells (WiCell)) were cultured on growth factor reduced Matrigel-coated (Corning) plates and daily supplemented with mTeSR1 medium (Stem Cell Technologies). The cells were then used to generate FBOs according to the STEMdiff Dorsal Forebrain Organoid Differentiation Kit (Stem Cell Technologies) with some modifications. In brief, on day 0, IMR90-4 cells were dissociated to single cells with Gentle Cell Dissociation Reagent (Stem Cell Technologies) and seeded in one well of an AggreWell 800 24-well plate at a final density of 10,000 cells per microwell ($3x10^6$ cells/Aggrewell) in 2 mL FBO Formation medium supplemented with 10 µM ROCK inhibitor (Sigma-Aldrich). On day 6 embryoid bodies (EBs) were transferred to low-adherent 24-well plates with 400 µL FBO Expansion Medium until day 11 where they were moved to low-adherent 6-well plates with 2 mL medium/well and placed on an orbital shaker at 57 rpm (INFORS HT Celltron) to avoid organoid fusions. From day 43 FBOs were supplemented with 100 U/mL of Penicillin-Streptomycin (Gibco, 15140) and 1 µg/mL of Amphotericin B (Thermo Fisher Scientific). FBOs were cultured for 100 days before applying the differential centrifugation workflow.
All cell and organoid cultures were maintained with 5% CO_2 at 37°C.

Generation of cerebral organoids and ALI-CO cultures

H9 (female) human embryonic stem cells were purchased from WiCell (WA09) and approved for use in this project by the UK Stem Cell Bank Steering Committee. Cells were maintained in StemFlex medium (Thermo Fisher Scientific) on plates coated with growth factor reduced Matrigel (Corning) and passaged twice weekly with EDTA.

Cerebral organoids were generated according to the STEMdiff Cerebral Organoid Kit (Stem Cell Technologies) seeding 2000 cells per EB. At 15 days *in vitro*, organoids were manually excised from the Matrigel droplets in which they were embedded during the kit protocol, using a needle and fine scalpel under a stereomicroscope, and returned to organoid media. From day 30, organoid media was supplemented with Matrigel (Corning) dissolved at 2% (v/v).

For culture at the air-liquid interface (ALI), cerebral organoids (CO) of day 55-60 were processed to 300 µm slices as previously described [66] and collected directly onto cell culture inserts (Millipore) with serum free slice culture medium beneath (SFSCM: Neurobasal (Thermo Fisher Scientific), 1x B-27 supplement (Thermo Fisher Scientific), 1x Glutamax (Thermo Fisher Scientific), 0.5% (w/v) glucose). SFSCM was supplemented with 1x antibiotic-antimycotic (Thermo Fisher Scientific) and additional 1:1,000 (v/v) Amphotericin B (Merck, A2942-20ML). Cell culture inserts were raised vertically within their respective wells using custom-manufactured stages (MRC LMB mechanical workshop) such that more SFSCM, approximately 4.5 ml, could fit beneath each insert, permitting twice-weekly full media changes.

All cell, organoid, and ALI-CO cultures were maintained with 5% CO_2 at 37°C.

Animal hold

Mouse brain tissue was obtained from 2-day-old C57BL/6J mice or 8 weeks old male C57BL/6J mice (Taconic or Janvier). Mice were housed in the Biomedical Laboratory at University of Southern Denmark (SDU) under a 12:12h light:dark cycle with food and water available ad libitum until use. C57BL/6J mice from Taconic were used for breeding mouse pups at the Biomedical Laboratory, SDU. Mice were euthanized by cervical dislocation and their brains were immediately dissected, removing the cerebellum from adult individuals. The brains were used for either the differential centrifugation enrichment workflow (2-day-old (P2) and 8-week-old adult tissue (W8)) or a standard Percoll enrichment procedure (only adult tissue) as described in the following.

Human cortical tissue

During surgery and after informed consent (approval ID S-20130048 from the Danish Research Ethics Committees), fresh human, non-tumorous (healthy and non-eloquent) cortical tissue samples were collected from healthy residual specimens obtained surgeries for high-grade gliomas conducted at Odense University Hospital (University of Southern Denmark, SDU). The tissues were directly collected in ice-cold phosphate-buffered saline (PBS) and immediately processed within one hour.

Serial differential centrifugation enrichment of synaptosomes

Mouse brains (8 weeks old or 2-day-old), FBOs, ALI-COs or surgery-derived fresh human cortical tissue were homogenized in ice cold sucrose/EDTA buffer (0.32 M sucrose, 1 mM EDTA, 5 mM Tris base, pH 7.4, using around 700-800 µL buffer/100 mg of tissue) applying 6 up-and-down strokes with a tissue grinder (15-ml Potter-Elvehjem type Teflon-glass tissue grinder, Wheaton) at 700 rpm. A homogenate aliquot of 100-200 µL was obtained and stored at -70°C as a reference/control sample for the enrichment. Then, the remaining homogenate was centrifuged at 800xg for 15 min at 4°C to pellet nuclei and cellular debris, and the centrifugation was repeated after redissolving the pellet (P1 fraction) in the half amount of sucrose buffer. The protein concentration of the supernatant (S1) was measured using a nanophotometer (N60, Implen), and the S1 fraction was split into 3 or 4 replicates of 1.5-3 mg of protein each. Dithiothreitol (DTT) was added to the samples to a final concentration of 0.25 mM before starting the differential centrifugations. Finally, samples went through the differential centrifugations, 5,000xg for 10 min, 12,000xg for 20 min, 22,000xg for 20 min, all at 4°C, and the pellets (P5,000, P12,000, P22,000) and the supernatant from the last centrifugation (S22,000, named the “cytosolic” fraction) were collected.

Standard Percoll gradient enrichment of synaptosomes from mice

Mouse brains were homogenized in sucrose/EDTA buffer following a standard Percoll density gradient synaptosome enrichment procedure [19]. Briefly, brains were homogenized with 6 up-and-down strokes at 700 rpm using a Teflon-glass tissue grinder (Wheaton) and kept on ice or at 4°C during the following procedure until stimulation. A homogenate aliquot (100-200 µL) was obtained

(stored at -70°C) as a reference/control for the enrichment and the remaining homogenate was centrifuged at 800xg for 10 min, the supernatant (S1) was obtained and DTT was added to a final concentration of 0.25 mM. Carefully, 2 mL of S1 was layered on top of each Percoll density gradient (4 layers of 3%, 10%, 15% and 23% Percoll (Cytiva) in sucrose/EDTA buffer with 0.25 mM DTT) and centrifuged at 20,000 rpm for 5 min when reaching top speed in a Sorval RC 5C plus Harvest centrifuge using a Sorval SS34 rotor. The F3 and F4 layers were collected and washed with sucrose/EDTA buffer followed by another centrifugation at 16,000 rpm for 15 minutes. The pellets were collected into low-binding Eppendorf tubes (Sorenson BioScience Inc.), centrifuged for 10 min at 950xg and the sucrose buffer was removed. Fractions for label-free proteomic analysis were stored at -70°C. F4 fractions were further washed in HEPES-buffered Krebs-like (HBK) control buffer (4.7 mM KCl, 118 mM NaCl, 20 mM HEPES, 1.18 mM $MgSO_4$, 1.2 mM $CaCl_2$, 0.1 mM Na_2HPO_4, 10 mM glucose, 10 mM pyruvate, 25 mM $NaHCO_3$, pH7.4, which had been bubbled with carbogen (95% O_2, 5% CO_2) for approx. 1 hour before use) and used for high KCl stimulation and phosphopeptide enrichment.

Stimulation of synaptosomal fractions with high KCl

Fractions from the differential centrifugation series and F4 fractions from Percoll enrichment were resuspended in 37°C HBK control buffer and incubated at 37°C for 1 h to allow regeneration of the resting membrane potential. Subsequently, 15 sec stimulation was performed by adding an equal volume of High KCl HBK buffer (147.7 mM KCl, 20 mM HEPES, 1.18 mM $MgSO_4$, 1.2 mM $CaCl_2$, 0.1 mM Na_2HPO_4, 10 mM glucose, pH7.4) resulting in a final concentration of 76.2 mM KCl. The stimulation was stopped by snap-freezing in liquid nitrogen and the samples were kept at -70°C until further use. Control samples were stimulated in the same way but with HBK control buffer.

Sample lysis and digestion of proteins

The sucrose/EDTA buffer from the enrichment protocols was removed from the homogenate samples and cytosolic fractions (S22,000) using 10 kDa spin filters (Amicon Ultra-0.5 Centrifugal Filter Unit) by centrifuging at 11,000xg for 20 min at 4°C. The samples were washed x2 with 300 µL of 50 mM triethylammonium bicarbonate (TEAB), pH 8. All fraction and homogenate samples were dissolved in lysis buffer (1% sodium deoxycholate (SDC) in either 50 mM TEAB or 100 mM HEPES, pH 8) in low-binding Eppendorf tubes (Sorenson BioScience Inc.). Samples were probe sonicated 3x10 sec at 40% amplitude on ice, centrifuged for 10 min at 14,000xg and the supernatants were transferred to new tubes. Protein concentrations were measured using a Nanophotometer (Implen). An aliquot of protein (10-20 µg for label-free DIA analysis and 50-70 µg for TMT-labeling and phosphopeptide enrichment) was prepared from each sample and the proteins were reduced with 10 mM DTT at room temperature (RT) for 20 min followed by alkylation with 20 mM iodoacetamide (IAA) for 30 min in the dark at RT. After alkylation, the IAA reaction was quenched by raising the DTT concentration to 15 mM. Samples were predigested with 0.04 active units/mg Lys-C for 1h at RT followed by overnight (ON) digestion with 5% trypsin (in-house, methylated trypsin

[72]) at 37°C, pH 8. The following day, samples were incubated 1h at 37°C with 1% additional trypsin.

Data independent acquisition (DIA) workflow using label-free quantification of proteins

After digestion, the SDC was precipitated using 2% formic acid (FA) followed by centrifugation and samples lyophilized and subsequently resuspended in 0.1% FA. Peptide concentrations were measured using Pierce Quantitative Fluorometric Peptide Assay (Thermo Fisher Scientific) according to manufacturer instructions and samples were diluted accordingly in 0.1% FA to a final concentration of 0.1 µg/µL.

Differential centrifugation fractions from FBOs, mouse (P2 and W8), human cortex and Percoll density gradient F3 and F4 fractions from adult mouse brain (W8) were analyzed the following way: a total of 2 µL (200ng of peptides) was loaded onto a 15 cm x 75 µm, C18 1.6 m Aurora Elite column (ESI Source Solutions) coupled directly to a TIMSTOF Pro (Bruker) instrument using buffers A (0.1% FA) and B (95% ACN, 0.1% FA). Peptides were eluted during a 30 min gradient (flow rate: 0.4 µL/min, increasing proportion of buffer B: from 0-2 min: 5%, from 2-18 min: 5-28%, from 18-22 min: 28-45%, from 22-23 min: 45-95%, from 23-26 min: 95%, from 26-26.5 min: 95-5%, from 26.5-30 min: 5%) on a Dionex Ultimate 3000 HPLC-system (Thermo Scientific). Samples were run scanning from 100-1700 m/z, operating in positive ion mode and using a standard DIA-PASEF method (mass range: 395.6 Da to 1020.6 Da, cycle time estimate: 1.06 sec).

The ALI-CO differential centrifugation fractions were analyzed in the same way with minor modifications in the gradient (30 min gradient at flow rate: 0.4 µL/min, increasing proportion of buffer B: from 0-2 min: 1%, from 2-2.5 min: 1-5%, from 2.5-18 min: 5-28%, from 18-22 min: 28-45%, from 22-23 min: 45-95%, from 23-26 min: 95%, from 26-26.5 min: 95-1%, from 26.5-30 min: 1%) and DIA-PASEF method (mass range: 400 Da to 1201 Da, cycle time estimate: 1.80 sec).

The mouse (2-day-old and adult) label-free proteomic samples were analyzed on an orbitrap Exploris 480 Instrument using a DIA method. A total of 200 ng of peptides were loaded onto a Vanquish™ Neo UHPLC system (Thermo Scientific) using a 2-column setup (Trap column of 0.5 cm, inner diameter: 300 µm and Separation column of 23 cm, inner diameter: 100 µm). Peptides were eluted with increasing amount of buffer B at a flow rate of 0.3 µL/min during a 35 min gradient: from 0-27 min: 2-29%, from 27-30 min: 29-42%, from 30-31 min: 42-70%, from 31-34 min: 70%, from 34-35: 70-100%. Peptides were analyzed using a standard DIA Scan method (precursor mass range (m/z): 400-1000, cycle time of 3 sec, orbitrap resolution: 30,000 full width half maximum (FWHM)).

Peptide identification and quantification of label-free samples

The raw data from DIA-MS analyses was searched with DIA-NN (v1.8.1) against computationally generated spectral libraries of human and mouse proteomes performed with the following search parameters: mass accuracy was set to 10 ppm whereas for MS1 mass accuracy to 15 ppm , peptide

length range of 7-30 amino acids, precursor m/z range of 100-1700, fragment ion m/z range of 100-1700, neural network classifier in Single-pass mode, Robust LC (high precision) mode was used with retention time (RT)-dependent normalization enabled, maximum of 2 missed cleavages, N-terminal methionine (M) excision and methionine oxidation as variable modification was enabled, C carbamidomethylation was used as fixed modification.

TMT-labeling of samples for phosphopeptide enrichment

After digestion, samples for phosphopeptide enrichment (high KCl stimulated fractions and controls) were labeled with isobaric Tandem Mass Tags (TMT) using TMTpro™ 16-plex or TMTpro™ 18-plex (Thermo Fisher Scientific) according to manufacturer instructions as follows: TMT-reagent (0.25 mg) for 50 µg of sample were thawed for 5 min with frequent vortexing in 100% acetonitrile (ACN). Reagents were mixed with 50 or 70 µg of peptides per sample in lysis buffer (1:5, ACN:sample v/v). The pH was adjusted to 8 with 1 M TEAB and the labeling reaction was allowed for 1-1.5 h at RT. Labeling efficiency and TMT intensities were tested by mixing 1 µL of each sample in 2% FA followed by centrifugation at 20,000xg for 10 min to precipitate the SDC. A test sample, using approximately 1 µg of the mixed sample, was run on LC-MS/MS using an orbitrap Exploris 480 instrument. The TMT labeled samples were mixed according to the obtained results from the test. The SDC was precipitated using 2% FA and pelleted with centrifugation (20,000xg for 10 min) and the combined sample was lyophilized until a remaining volume of 100 µL, which was then used for TiO_2 enrichment of phosphopeptides.

TiO_2 enrichment of phosphopeptides

The enrichment of phosphopeptides was performed from the TMT labeled peptide mixture by using TiO_2 [73, 74]. This highly efficient method utilizes TiO_2 enrichment in the presence of Glycolic acid, trifluoracetic acid (TFA) and acetonitrile (ACN) which dramatically prevent binding of non-phosphorylated peptides to TiO_2 [74].

After binding of the phosphopeptides to the TiO_2 resin (GL Sciences, Japan) in 5% TFA, 80% Acetonitrile (ACN) and 1M Glycolic acid for 10 min, the solution was centrifuged, and the supernatant was re-incubated with half the amount of TiO_2 for another 10 min. The supernatant from the second incubation was collected, labeled as “non-modified” proteins and dried for further use (protein expression). The TiO_2 resin from the two incubations were washed using 200 µL loading buffer, 200 µL 80% ACN, 1% TFA and 100 µL 10% ACN, 0.5% TFA, respectively. After the final wash, the beads were lyophilized for 5 min and subsequently the phosphopeptides were eluted with 5% ammonia water, pH 11. After incubation, the supernatant was collected and lyophilized without TiO_2 beads for subsequent high pH reversed phase fractionation.

Desalting of “non-modified” peptides

The flow-through from the TiO_2 enrichment was dried and subsequently resolubilized in 2 mL 0.1% TFA. The peptides were desalted on a Waters™ Oasis HLB Cartridge. The HLB cartridge was washed

with 2 mL 100 % Methanol followed by 2 mL 100 % ACN using a 5 mL syringe. The HLB resin was equilibrated with 2 mL 0.1% TFA and the sample was loaded slowly using the 5 mL syringe. The HLB cartridge was washed with 2 mL 0.1% TFA and the peptides were eluted with 1 mL 50% ACN in water and subsequently the HLB cartridge was washed with 1 mL 70% ACN. Both elutions were lyophilized and stored until further use.

High pH reversed phase (RP) fractionation

The "non-modified" peptide and phosphopeptide samples were dissolved in high pH RP fractionation solvent A (20 mM ammonium formate, pH 9.3) and pH was adjusted with 1 M TEAB to around 9. Samples were fractionated on a Dionex Ultimate 3,000 HPLC system (Thermo Fisher Scientific) using an Acquity UPLC®-Class CSHTM C18 column (Waters) into 15 concatenated fractions with the following gradient of solvent B (80% ACN and 20% buffer A): sample loading with 2% solvent B, peptide elution (and fraction collection every 122 sec) from 2-50% in 59 min, 50-70% in 10 min, 70-95% in 5 min and for 10 min at 95% solvent B (during which collection of fractions was terminated). Flow rate was 5 µL/min. Fractions were lyophilized and resuspended in 0.1% FA for LC-MS/MS analysis.

Data Dependent Acquisition (DDA) Nano Liquid Chromatography-Electrospray-Tandem Mass spectrometry (nLC-ESI-MS/MS)

All samples were dissolved in 0.1% FA and analyzed by nano LC-ESI-MS/MS using an EASY-nLC (Thermo Fisher Scientific) with buffer A (0.1% FA) and buffer B (95% ACN, 0.1% FA) connected online to an Orbitrap Eclipse Tribrid Mass Spectrometer (Thermo Fisher Scientific, USA). The separation was performed on an in-house made fused silica capillary two-column setup, a 3 cm pre-column (100 µm inner diameter packed with Reprosil-Pur 120 C18-AQ, 5 µm (Dr. Maisch GmbH)) and an 18 cm pulled emitter analytical column (75 µm inner diameter packed with Reprosil-Pur 120 C18-AQ, 3 µm (Dr. Maisch GmbH)). The peptides were eluted with increasing amount of the buffer B (95% ACN, 0.1% FA) from 2 to 40% in 90 and 140 min for phosphopeptide fractions and "non-modified" peptides, respectively. All spectra were generated using DDA acquisition with positive ion mode mass spectrometry. The full MS was performed in the mass range of 450–1500, in the Orbitrap with a resolution of 120,000 FWHM, a maximum injection time of 50 ms and an Automatic Gain Control (AGC) target value of $1x10^6$. Hereafter, the peptides were selected for MS/MS using higher energy collision dissociation (HCD) with normalized collision energy (NCE) setting as 35, resolution of 50,000 FWHM, AGC target value of $1x10^5$ ions and maximum injection time of 150 ms. Additionally, the "non-modified" samples were run on the Eclipse Orbitrap in TMT SPS-MS3 mode with real-time search [75] enabled against a Uniprot human/mouse protein database (static modifications: carbamidomethyl (C), TMTpro™ 16- or 18-plex (Kn), maximum missed cleavages: 1) with a maximum search time of 35 ms. The MS/MS isolation window was set to 2 m/z and peptides with confident identification using the build-in search engine were selected for MS3 fragmentation

using HCD with NCE setting at 55, Orbitrap resolution of 30,000 FWHM, AGC target value of 500% with a scan range of 100-500 m/z.

Peptide Identification and quantification of "non-modified" peptide and phosphopeptide samples

All raw files were searched against the Uniprot database of Homo sapiens or Mus Musculus in Proteome Discoverer (PD) 2.5.0.305 (Thermo Fisher Scientific, USA) using an in-house Mascot server (v2.6) and SEQUEST HT.

For HCD fragmentation, search parameters were as following: cleavage specificity Trypsin/P; precursor mass tolerance of 10 ppm and fragment mass tolerance of 0.05 Da. The phosphopeptides search included the parameters: Maximum missed cleavages, 2; Static modifications, TMTpro (K), TMTpro (N-term) and Carbamidomethyl (C); Dynamic modifications, Phosphorylation (S, T, Y). For SPS-MS3 of "non-modified" peptides, the data were searched in PD 2.5.0.305 using SEQUEST with the same Uniprot Human/Mouse database as the real time search on the Eclipse. Search parameters were as following: cleavage specificity Trypsin/P; precursor mass tolerance of 10 ppm and fragment mass tolerance of 0.8 Da. The search included the parameters: Maximum missed cleavages, 2; Static modifications, TMTpro (K), TMTpro (N-term) and Carbamidomethyl (C). For the phosphopeptides the search was performed first in Mascot and then in SEQUEST using the same Uniprot databases and same search parameters, except for 0.05 mass tolerance in MS2 data and variable phosphorylation on S/T/Y.

The percolator software in PD 2.5 was used for filtering for false discovery rate (FDR) of <1% for proteins and peptides. All datasets from PD 2.5 were exported to Excel (Microsoft) for further processing. For the Mascot searches peptides were accepted if the Mascot score was ≥15.

Statistical analysis and data processing

Statistics of the proteomic datasets, TMT-labeled phosphopeptide data as well as label-free datasets (all log2 transformed) was performed with the online available PolyStest [76], using the final PolyStest FDR values, except for one dataset applying the Limma FDR - both with Benjamini-Hochberg-based correction for multiple testing. Before statistical analysis, all label-free DIA datasets were sorted to obtain a maximum of 25% missing values for each protein across the whole dataset. Regulations in label-free datasets were considered significant when FDR ≤ 0.01 and fold change ≥ 1.5 up or down. Regulations in TMT-labeled datasets (phosphopeptides) were considered significant when FDR ≤ 0.05 and fold change ≥ 1.3 up or down, except for the ALI-CO day 150 data (FDR ≤ 0.2 and FC ≥ 1.3 up or down). "Non-modified" TMT-labeled data was used only for identification of background protein lists for Gene Ontology (GO) term enrichment analyses.

Protein-protein interaction (PPI) networks and GO term enrichment analyses (Cellular component (CC), Biological Process (BP) and Molecular Function (MF)) were performed in Cytoscape (v3.10.0) applying the StringApp [77] using confidence score cutoff 0.7 or 0.4 for the PPI-networks (only connected nodes) and filtering for redundant terms in GO term enrichment analysis (cutoff: 0.4).

Full lists of identified proteins per dataset were used as background for each enrichment analysis, e.g., the full list of proteins identified from the FBO fractions dataset was used as background for the GO term enrichment analysis of FBO fractions etc. For the phosphopeptide datasets, all identified master proteins in “non-modified” (based on > 2 unique peptides) and phosphopeptide datasets combined were used as background (one list per TMT-set) for the enrichment analysis. The Cytoscape OmicsVisualizer [78] app was used to display significant changes in phosphopeptide sites.

Dot plots, principal component analysis (PCA) plots, correlation plot and bar-graphs were made in R (v4.3.0) [79] using the package ggplot2 [80] and ChatGPT (vAugust 3, 2023) was used, for coding assistance. Heatmaps were made using the pHeatmap package [81] in R.

The statistical test used for changes in synaptic and growth cone marker proteins was a Wilcoxon Rank Sum test, suited for data where normal distribution and equal variance cannot be assumed. Tests were conducted as one-sided, testing for up-regulation in P5,000, P12,000 and P22,000 fractions and down-regulation in Cytosolic fractions.

Immunofluorescent labeling

Organoids were fixed with 4% paraformaldehyde (Thermo Fisher Scientific) in PBS (Gibco) for 1 h at RT and soaked in 30% sucrose in PBS ON or until further processed. Organoids were embedded in OCT mounting media (VWR), snap frozen in < -50°C ethanol and sectioned in 30 µm sections on a Leica CM1860 cryostat at -17 to -20°C. Sections were placed on microscope slides (Thermo Fisher Scientific) and stored at -20°C.

Slices were hydrated with PBS and washed 2x5 min with wash buffer (0.1% TritonX100 (Plusone) in PBS). Permeabilization and blocking buffer (5% donkey serum (BioWest)) was added followed by 30 min incubation at RT. Primary antibodies diluted in wash buffer incl. 1% donkey serum (BioWest) were added (see dilutions in **Table 1**) and slices were incubated ON at 4°C to allow binding. Slices were washed in wash buffer for 3x10 min followed by incubation for 1 h in the dark with secondary antibodies diluted in wash buffer and 1% donkey serum (see dilutions in **Table 2**). Secondary antibodies were removed, and slices were washed with PBS for 3x10 min followed by mounting with DAPI-containing ProLong Diamond Antifade mountant (Invitrogen). The slices were stored in the dark at 4°C until image acquisition.

The images were obtained with confocal microscopy on a Nikon A1R confocal unit coupled to a Ti-2 LFOV microscope. Images were analyzed with ImageJ (v1.53t).

Table 1: Primary antibodies for labeling of synapses in FBO slices

Antigen	Species	Company	Cat. No.	Dilution
MAP2	mouse	Sigma	M1406	1:2000
PSD95	goat	Abcam	ab12093	1:100
SYP	mouse	Merck Millipore	S5768	1:200
SYN1	rabbit	Abcam	ab254349	1:500
VGLUT1	rabbit	Synaptic Systems	135303	1:1000

Table 2: Secondary antibodies for labeling of synapses in FBO slices

Secondary antibody	Company	Cat. No.	Dilution
Alexa Fluor 488 donkey-anti-mouse IgG (H+L)	Life Technologies	A21202	1:5000
Alexa Fluor 647 donkey-anti-rabbit IgG (H+L)	Life Technologies	A31573	1:500
Alexa Fluor 568 donkey-anti-goat	Life Technologies	A11057	1:1000

Transmission electron microscopic (TEM) analysis

Fractions were fixed in 3% glutaraldehyde in 0.1 M sodium phosphate (SP) buffer (78mM Na_2HPO_4, 22mM NaH_2PO_4, pH 7.3) for 0.5-1 h on ice. The fixing solution was replaced with 0.1 M SP buffer and samples were stored at 4°C until further processing. The fractions were embedded in 4% Batco agar at 45°C (BD diagnostics) and washed x2 in 0.1 M SP buffer. The samples were postfixed in 1% OsO4 (in 0.1 M SP buffer) for 1 h at RT and covered in folio followed by washing x2 in Milli-Q water. The samples were subsequently dehydrated in a series of increasing concentrations of ethanol (EtOH): 50% EtOH (10 min), 70% EtOH (10 min), 96% EtOH (10 min) and 99% EtOH (3×20 min). The EtOH series was followed by an intermediate solution of propylene oxide (Merck) (2×10 min). Samples were then gradually infiltrated in Epon (812 Resin, TAAB T031) and incubated in a rotor ON in pure Epon. Next, the samples were embedded in Epon and polymerization was allowed for 48 h at 60°C. The specimens were cut in semi-thin sections of 2 µm with a glass knife (LKB Bromma 7800, Leica Microsystems) on an ultramicrotome (Reichert Ultracut S, Leica, Microsystems) followed by staining with 1% toluidine blue (VWR) in 0.1% Borex (VWR), to identify a section of interest. Ultra-thin sections of 50–60 nm were cut with a diamond knife (MD1035) on an ultramicrotome (Reichert Ultracut S, Leica, Microsystems) and collected on 150 mesh copper grids (Gilder) and coated with a parlodion-amyl acetate film (EMS). Finally, the sections were contrasted using 2% uranyl acetate (Polyscience, 21447) and 1% lead citrate (Reynold, 1963).

The micrographs were examined with a Talos L120C transmission electron microscope operating at 80 kV and images were acquired using a Ceta camera and Velux software (Olympus).

Western blotting

Samples were lysed in 1% SDC and 50 mM TEAB, pH 8, and sonicated 3x10 sec on ice at 40% amplitude. Following sonication, samples were centrifuged at 14,000xg for 10 min at RT and supernatant transferred to new Eppendorf tubes (Sorenson BioScience Inc.). Protein concentration

was determined by Nanophotometer (Implen). For each sample 3.2 µg protein was separated using Bolt 4-12% Bis-Tris Plus Gels (Thermo Fisher Scientific) with samples loaded in NuPage LDS Sample buffer (Thermo Fisher Scientific) with NuPage Sample Reducing agent (Thermo Fisher Scientific) and PageRuler Plus pre-stained protein standard (Thermo Fisher Scientific) for size reference. Proteins were transferred to activated PVDF membranes (Millipore) using the Trans-Blot® Turbo™ Transfer System (BioRad) and membranes were blocked with 5% skimmed milk in TBS-Tween20 (TBST) buffer for 1 h and incubated overnight at 4°C in 5% milk/TBST with the following primary antibodies: Anti-rabbit TOMM20 (Abcam) 1:1,000 or mouse anti-Synaptophysin (SYP, Millipore) 1:200. Anti-mouse β-actin HRP-linked (Abcam) 1:50,000 was used as loading control. Following 3 x wash in TBST, the membranes were incubated for 2 h at RT in TBST with the following secondary antibodies: anti-rabbit IgG, HRP-linked (Cell signalling) 1:10,000 or anti-mouse IgG, HRP-linked (Abcam) 1:10,000. Following 3 x wash in TBST, the membranes were visualized with Immobilon ECL Ultra Western HRP Substrate (Millipore) using an Amersham 680 Imager (GE Healthcare).

Results

The differential centrifugation protocol shows high reproducibility between different brain tissue types

Differential centrifugation strategies have previously been used in combination with TMT-based proteomics to characterize organelle-specific proteins in various cell types. A study from 2019 by Geladaki et al. observed mitochondrial pelleting at 3,000xg, Peroxisomes at 5,000xg, lysosomes at 12,000xg and Golgi and ER from 15,000-30,000xg [67]. Based on an estimated density of synaptosomes, we expected these structures to be pelleted around 5,000-12,000xg. The developed workflow for differential centrifugation enrichment of synaptic structures from human NOs is shown in **fig. 1C**. To test the applicability of the differential centrifugation protocol for enrichment of synaptosomes, the protocol was applied to two types of neural organoids (FBOs at day 100 and ALI-COs at day 90 and 150 (**fig. S1A**)) together with newborn (postnatal day 2, P2) and adult (week 8, W8) mouse brain and adult human cortical tissue (surgery derived, healthy tissue). Prior to the enrichment, the presence of synapses in the neural organoid tissues was confirmed with IHC labelling of pre and postsynaptic markers (SYN1, VGLUT1, SYP, PSD95 and MAP2), showing co-localization in both organoid types (**fig. S1B-D**). Furthermore, a standard procedure for enrichment of synaptosomes, based on discontinuous Percoll density gradient centrifugation [19], was performed in parallel on adult mouse brain (W8) for comparison. The Percoll-based synaptosome enrichment generated the synaptosome-containing fractions F4 and F3 and the pellet from the first 800xg centrifugation (P1) was used as a negative reference for synapse specific proteins for the Percoll enrichment procedure. The differential centrifugation workflow generated the following samples: Homogenate (H), three pellets from each round of centrifugation (fractions P5,000, P12,000 and P22,000) and finally the remaining supernatant, which will be referred to as the Cytosolic fraction. For each tissue type, four technical replicates of the differential centrifugation were generated. All differential centrifugation fractions and the standard Percoll synaptosome-enrichment fractions, were examined with LC-MS/MS-based proteomics using a label-free DIA (data independent analysis) approach for quantification. Principal component analyses (PCA) of the proteomic results from the differential centrifugation method showed very similar patterns of fraction distribution suggesting high reproducibility between the different tissue types (**fig. 1D**).

Evaluation of protein content from the differential centrifugation fractions

For all differential centrifugation fractions from each tissue type the significantly increased (fraction-specific) proteins compared to H (FC ≥ 1.5 and FDR < 0.01) were extracted and subjected to GO cellular component (CC) enrichment analysis using whole datasets (all identified proteins) as background. **Fig. 2** shows a summary of the GO CC terms enriched in the differential centrifugation fractions from FBOs, ALI-COs day 90, mouse P2, and adult human cortex. The top 20 enriched GO CC terms (FDR < 0.05) for each tissue type can be found in supplementary **fig. S2A-P** and **S3A-D**.

For all tissue types, the P5,000 fractions mainly showed enrichment of mitochondrial proteins and associated terms. However, the term “Presynapse” (FDR: 1.66E-5, 98 proteins out of 351 in the background) was among the top 20 in the FBO P5,000 fraction and two other synaptic terms “Presynaptic membrane” (FDR: 0.0014, 35 proteins) and “Synaptic vesicle membrane” (FDR: 0.0022, 29 proteins) were also enriched, but not part of the top 20. Furthermore, the term “Secretory vesicle” was enriched in FBO P5,000 (FDR: 0.0496) based on 116 fraction-specific proteins out of 560 annotated background proteins. Collectively they suggested some enrichment in pre-synaptic structures. On the other hand, the P5,000 fraction-specific proteins from ALI-COs at day 90 and the human cortex P5,000 only showed enrichment in mitochondrial terms among the top 20.

The P12,000 fractions generally showed enrichment in several synaptic GO CC terms together with mitochondrial proteins, some lysosomal and peroxisomal proteins and general membrane-related terms (**fig. 2** and **S2B, F, J, N** and **S3B**). Notably, some enrichment in mitochondrial proteins is expected in synaptosome preparations, as mitochondria are essential for functional synaptosomes. The significantly enriched terms of the FBO P12,000 comprised e.g., the terms “Presynapse” (FDR: 5.40E-10, 136 proteins out of 351), “Postsynaptic membrane” (FDR: 5.64E-10, 83 proteins out of 166), “Glutamatergic synapse” (FDR: 4.52E-5, 92 proteins out of 267), “Synaptic vesicle membrane” (FDR: 0.0127, 30 proteins out of 76), “Presynaptic active zone membrane” (FDR: 0.0498, 12 proteins out of 22) and other synapse-related terms, together building a picture of both pre-and post-synaptic structures as expected in a synaptosomes. The ALI-CO day 90 P12,000 fraction showed e.g. enrichment in the terms “Neuron projection” (FDR: 1.58E-14, 109 proteins out of 615), “Postsynaptic specialization” (FDR: 6.34E-11, 54 proteins out of 220) and “Presynaptic membrane” (FDR: 3.86E-9, 30 proteins out of 82). Interestingly, the P12,000 and P22,000 fractions from ALI-COs day 90 had more synapse related terms among the top 20 enriched GO CC terms compared to the same fractions from FBOs (**fig. S2B-C** and **F-G**). The human cortex P12,000 fraction-specific proteins showed enrichment in terms like “Intrinsic component of synaptic membrane” (FDR: 5.09E-8, 26 proteins out of 108), “Presynapse” (FDR: 1.91E-5, 43 proteins out of 355) and “GABA-ergic synapse” (FDR: 1.90E-4, 14 proteins out of 57). The human P12,000 fraction furthermore showed enrichment in voltage gated ion channels as indicated by the terms “Voltage-gated calcium channel complex” (FDR: 0.0032, 7 proteins out of 18 annotated in the background), “Voltage-gated potassium channel complex” (FDR: 0.0066, 8 proteins out of 29) and “Voltage-gated sodium channel complex" (FDR: 0.0108, 4 proteins out of 5), which are essential for neuronal signaling and synaptic transmission.

The P22,000 fraction-specific proteins were enriched in several synaptic terms similar to the P12,000 fractions (**fig. 2** and **S2C, G, K, O** and **fig. S3C**). However, they also showed a substantial enrichment in membrane related terms including the endomembrane system, such as “Endoplasmic reticulum membrane” and “Golgi apparatus”. No mitochondrial terms were enriched in these fractions. The Cytosolic fraction-specific proteins were enriched in GO CC terms mainly related to the cytosol and nucleus for both tissue types, the latter indicating content from nuclei that were broken at homogenization (**fig. S2D, H, L, P** and **S3D**).

Overall, the differential centrifugation fractions showed a very similar pattern of enrichment in GO CC terms. To confirm the mitochondrial distribution in the fractions, we conducted western blots (WBs) of the mitochondrial marker TOMM20 on the FBO and human cortex samples (**fig. S3E**). Correspondingly, the WBs showed a high level of Tomm20 in the P5,000 fractions and steadily declining levels in the P12,000, P22,000 and Cytosolic fractions for all 3 technical replicates in both tissue types.

Enrichment of synaptic proteins by differential centrifugation

To investigate the more detailed composition of the fractions, 30 proteins mainly located in synapses and present in most of the analyzed datasets (the ALI-CO day 90 dataset had only 26), were selected for analysis. The levels of the selected synaptic proteins in each fraction were compared to the levels in the corresponding homogenate samples and their log2 fold changes (Log2FCs) were plotted for each tissue type including the synaptosome fractions from the traditional enrichment method (**fig. 3A**). The 30 selected synaptic proteins were not sorted for individual significance prior to the analysis. The overall tendency showed a significant increase of the selected synaptic proteins in all the pellet fractions (P5,000, P12,000 and P22,000), except for P22,000 in the adult human and mouse tissues. One-sided Wilcoxon Rank Sum test was used to test for significance of enrichment since normal distribution could not be assumed for the distribution of the synaptic proteins in the different fractions. For the young tissue types (FBOs, ALI-COs day 90 and Mouse P2) the enrichment was highest in the P12,000 and P22,000 fractions with fold changes (FCs) that were very similar to those of the F4 and F3 synaptosome-containing fractions from the standard Percoll-based method (see **table 3**). The FBO and Human Cortex P5,000 fractions also showed a similar enrichment. Thus, the relative amount of enrichment was comparable to the standard protocol and corresponds to an increase in synaptic protein amounts of around 40-50% in the highest enrichments of the P5,000 and P12,000 fractions. In the P22,000 fractions, the enrichment was around 50-70% in the younger tissues (FBO, ALI-CO day 90 and mouse P2), whereas the adult tissue P22,000 fractions (human cortex and mouse W8) did not show significant differences compared to the H samples. However, the P22,000 fractions also showed a larger variation between the individual synaptic protein Log2FCs with a clear tendency of some of these going down compared to P12,000 fraction Log2FCs (**fig. 3A**). The Cytosolic fractions all showed a significant decrease in the synaptic protein content indicating that a large part of the synaptic proteins had been pelleted in the previous fractions.

*Table 3: Average fold changes of the 30 selected synaptic proteins for each tissue type (26 for ALI-COs) as compared to their homogenates. *Non-significant p-value. The remaining p-values are below 0.01. P2: postnatal day 2, W8: week 8, FBO: dorsal forebrain organoid, ALI-CO: Air-liquid interface cerebral organoid, D: day.*

Fraction	Tissue type					
	FBO (D100)	ALI-CO (D90)	Human cortex	Mouse (P2)	Mouse (W8)	Mouse Percoll
P5,000	1.48	1.24	1.43	1.26	1.14	*NA*
P12,000	1.55	1.38	1.39	1.51	1.32	*NA*
P22,000	1.58	1.50	1.17*	1.67	1.08*	*NA*
Cytosolic	0.46	0.36	0.43	0.50	0.33	*NA*
F3	*NA*	*NA*	*NA*	*NA*	*NA*	1.52
F4	*NA*	*NA*	*NA*	*NA*	*NA*	1.43

A more detailed view of changes in the individual synaptic proteins is presented in **fig. 3B** showing heatmaps of the normalized protein abundances for each of the 30 (or 26 for ALI-CO day 90) synaptic proteins per fraction and tissue type. The proteins were sorted as mainly presynaptic or postsynaptic. The younger tissue types (FBO, ALI-CO day 90 and mouse P2) showed a trend of higher abundances of postsynaptic proteins in the P22,000 fractions compared to the P5,000 and P12,000 fractions. The presynaptic proteins, which are expected to be the main content of synaptosomes, were mainly increased in the P5,000 and P12,000 fractions of the FBO, ALI-CO and mouse P2.

Additionally, a WB of the synaptic marker synaptophysin (SYP) showed increased presence especially in the P5,000 and P12,000 fractions compared to H in both FBOs and human cortex fractions (**fig. 3C**). As expected, the human cortex fractions showed significantly higher levels of SYP compared to the FBO fractions.

Enrichment of growth cone markers with the differential centrifugation workflow

Since the neural organoid tissues are generally considered to be at early developmental stages, they are expected to harbor immature synapses and developing axons led by growth cones [71]. Growth cone particles (GCPs) – membrane-enclosed growth cones [82], have previously been enriched with density gradient-based methods like those used for synaptosomes [82-84]. We therefore explored the distribution of growth cone proteins in the fractions, based on growth cone markers as reported previously in two proteomic studies [85, 86]. Selected markers of growth cones (n=29) were extracted from the data and Log2FCs for each fraction were plotted for each of the

young tissue types (mouse P2, FBOs and ALI-COs day 90) (**fig. 4A**). The individual markers were not sorted for significance, however, the overall tendency showed significant enrichment of growth cone proteins in all three fractions (P5,000, P12,000 and P22,000) and significant depletion in the Cytosolic fractions (statistical test used: one-sided Wilcoxon Rank Sum test, applicable for non-normal distributed data). The enrichment of growth cone proteins from the organoids was highest in the P12,000 fractions with 41-46% enrichment (see **table 4**). For the P2 mouse fractions, P22,000 had the highest enrichment (46%) however with a higher variation and some growth cone protein levels starting to go down. Thus, when also considering the variation of the growth cone proteins, the P12,000 fraction shows the best enrichment. Looking into the well-characterized growth cone marker, Growth associated protein 43 (GAP43) [87], we furthermore saw significant enrichment in P12,000 of all the young tissue types, however, with peaking levels in the P22,000 fractions from ALI-COs day 90 and P2 mouse (**fig. 4B-C**).

Table 4: Average fold changes of the 29 selected growth cone proteins for each tissue type as compared to their homogenates. All p-values are below 0.01. P2: postnatal day 2. FBO: dorsal forebrain organoid, ALI-CO: Air-liquid interface cerebral organoid, D: day.

Fraction	Tissue type		
	FBO (D100)	ALI-CO (D90)	Mouse (P2)
P5,000	1.29	1.23	1.13
P12,000	1.41	1.46	1.26
P22,000	1.30	1.46	1.42
Cytosolic	0.54	0.50	0.63

TEM evaluation of synaptosome structures in the differential centrifugation fractions

Successful stimulation and depolarization of synaptosomes require intact membrane-enclosed synaptosomes. To verify that the differential centrifugation pellets contain structurally preserved synaptosomes, the P5,000, P12,000 and P22,000 fractions from human cortex, adult mouse and ALI-CO differential centrifugations were examined with TEM. Synaptosomes containing mitochondria and synaptic vesicles were clearly observed in the adult P5,000 and P12,000 fractions from both human and mouse (**fig. 5A-B** and supplementary **fig. S4A-B** and **D-E**). Some of these synaptosomes also showed electron dense AZs with PSD attached (**fig. S4A** and **D**). The ALI-CO P5,000 and P12,000 fractions at day 90 showed a few small synaptosome-like structures. However, more explicitly the day 90 ALI-CO fractions contained membrane-enclosed structures with fibrous content, larger vesicles, and mitochondria (**fig. 5C-D** and **S4F-G**) resembling what earlier studies have defined as GCPs [82-84]. The described significant enrichment of growth cone markers

including GAP43 in the ALI-CO fractions (**fig. 4A-B**) further supports this notion. The P5,000 and P12,000 fractions from day 150 ALI-COs contained intact synaptosomes with mitochondria and synaptic vesicles, though the number of vesicles was smaller than in mature synaptosomes. Thus, we refer to these as immature synaptosomes since early in synaptogenesis, fewer vesicles are present in the synaptic bouton [88]. Both the P5,000 and the P12,000 fractions contained non-synaptic mitochondria (e.g., **fig. S4A, D** and **F**). The P22,000 fractions (**fig. S4C** and **J**) contained mostly smaller membrane structures in line with the proteomic GO CC enrichment profile that showed enrichment in endomembrane system and general membrane terms.

Synaptosomes enriched from adult mouse with differential centrifugation show stimulation-related changes in protein phosphorylation

KCl stimulation of synaptosomes is known to cause depolarization-induced changes in protein phosphorylation [49-51]. To test whether such changes can be detected in synaptosome fractions enriched with differential centrifugation, stimulation was conducted with 76.2 mM KCl on all differential centrifugation pellet fractions enriched from adult mouse brain. All fractions were stimulated in 4 technical replicates and analyzed with TMT-based quantitative proteomics and phosphoproteomics as previously described [89]. The stimulation resulted in significant regulations (FC ≥ 1.3 up or down, FDR ≤ 0.05) in 33 phosphopeptides in the P5,000 fraction, while only a few were regulated in the P12,000 (9 phosphopeptides) and P22,000 fractions (3 phosphopeptides).

Protein-protein interaction (PPI) networks and regulated phosphosites for each protein are shown in **fig. 6A** for the P5,000 fraction (confidence score set to "high": 0.7, only connected nodes are shown). A GO CC and biological process (BP) enrichment analysis was made for the proteins showing regulations in phosphopeptides using all identified proteins including "non-modified" proteins for each TMT set as background. The analysis showed substantial enrichment in terms related to synapses and synaptic transmission for the P5,000 fraction (**fig. 6B-C**, only top 10 enriched terms are shown, FDR ≤ 0.05). For example, the term "Neurotransmitter secretion" was the top enriched GO BP (FDR: 4.20E-4, with 7 proteins). For the P12,000 fraction, the term "Synaptic vesicle clustering" was enriched (FDR: 0.0047, with 3 proteins) (**fig. 6C**). Furthermore, several key synaptic proteins, which play active roles in synaptic transmission showed changes in phosphorylation in both the P5,000 and P12,000 fractions such as BSN, PCLO, SYN2 and SYN3 and additionally, SYN1, DNM1 and ERC2 for the P5,000 fraction. Two well-studied phosphosites that are known to go down upon neurotransmitter release are the S774 and S778 of DNM1, which is active in synaptic vesicle endocytosis [90]. These sites were downregulated in the P5,000 fraction (**fig. 6A**). The two AZ proteins PCLO and BSN showed regulated phosphosites in both P5,000 and P12,000, but not in P22,000. These proteins have several known phosphosites, many of which have been shown to change during KCl stimulation-induced depolarization of synaptosomes [49, 51]. The BSN phosphosites S241 and S245 were downregulated in the P5,000 fraction, which has also been observed in two other studies of KCl stimulation-related changes in protein phosphorylation in synaptosomes [49, 51].

KCl stimulation of day 90 ALI-CO differential centrifugation fractions induces changes in protein phosphorylation related to neurodevelopment

Here, the key application of synaptosomes isolated from NOs was to study depolarization-induced changes in the synaptosomal phosphoproteome to characterize molecular mechanisms underlying release of neurotransmitters in human neurons. Although invaluable for studying protein dynamics, phosphoproteomics requires a significant amount of starting material to obtain a high coverage of the phosphorylation sites in synaptic proteins. Even though we used almost 160 FBOs and obtained good synaptic protein enrichment, we did not detect any changes in phosphorylation after KCl stimulation (n=3, data not shown) probably due to too little starting material. However, synaptosomes enriched by differential centrifugation from ALI-CO cultures at day 90 (43 slices derived from 6 cerebral organoids sliced at day 55) or day 150 of differentiation, provided enough material for stimulation and phosphoproteomic analysis. We observed a general tendency of the ALI-COs to yield higher protein content in the first supernatant (S1), offering more material for distribution into the following fractions (supplementary **fig. S4K-L**). Especially the number of organoids needed from the start of the study (supplementary **fig. S4L**) was much lower, when the cerebral organoids were sliced at day 55 and cultured as ALI-COs, as opposed to using the FBO, spherical culture protocol. However, this trend did not reach statistical significance with a limited number of replicates applied in this study (n=3 or 4, two-sided t-test p-value: 0.135).

High KCl stimulation (15 seconds) was applied to the P5,000 and P12,000 differential centrifugation fractions from day 90 ALI-COs. Phosphopeptides were enriched and analyzed with MSMS using TMT-labeling for quantification.

The TMT-based phosphoproteomic analysis identified 4,210 phosphopeptides from 1,575 proteins whereof 103 phosphopeptides from 82 proteins were found regulated in the P5,000 fraction and 171 phosphopeptides from 133 proteins were regulated in the P12,000 fraction (FC ≥ 1.3 up or down, FDR ≤ 0.05). PPI STRING networks are shown in **fig. 7A-B** for the proteins with regulated phosphopeptides and their regulated sites are indicated (confidence score cutoff: 0.7, only connected nodes are shown). A GO enrichment analysis, using the combined identified proteins from the “non-modified” and phosphopeptide datasets as background, showed enrichment in one GO CC term “Cytoskeleton” (FDR: 0.0046, 42 proteins out of 1122 in the background) for the P12,000 fraction proteins with regulated phosphorylation. No GO terms were significantly enriched in the P5,000 fraction. However, 27 proteins annotated to the “Cytoskeleton” term also showed phosphopeptide regulations in the P5,000 fraction out of a total of 80 proteins with regulated phosphorylation.

To further examine which types of proteins the significant phosphorylation changes occurred in, the proteins with phosphosite regulation from each fraction were categorized into various selected GO BP and CC terms according to the protein GO annotations (**fig. 7C**). Many proteins were involved in cytoskeletal and neurodevelopmental processes including proteins related to cell junctions, localization, synapses, growth cones, and neurite outgrowth.

To examine whether the two fractions (P5,000 and P12,000) reacted in a similar way to the KCl stimulation, the correlation of Log2FCs of significantly regulated phosphopeptides, detected in both P12,000 and P5,000 (n=59), was examined. **Fig. 7D** shows a correlation plot of the Log2FCs of these phosphopeptides revealing a high correlation (Pearson's correlation coefficient: 0.944, p-value: 3.58E-29) between the phosphopeptide regulations indicating that the two independently stimulated fractions reacted with a highly similar phosphorylation profile upon KCl stimulation.

Cytoskeleton and neurite outgrowth-associated proteins show changes in phosphorylation

Several hits from our phosphoproteomics experiment were cytoskeleton proteins known to be involved in neuronal development, axonogenesis and synaptogenesis and in this section, we are going to focus on them in more detail. The protein MAP1B is highly expressed during neuronal and axonal development and phosphorylated forms are known to be concentrated in the distal region of the growing axons, close to the growth cone [91, 92]. It is involved in microtubule dynamics and is important for axonal growth [93, 94]. MAP1B showed upregulation of phosphorylation at the sites S891 and T908 in both the P5,000 and P12,000 fractions after KCl stimulation (**fig. 7A-B**). Another protein, which is not annotated in the "cytoskeleton" term but is also involved in axonal outgrowth and stabilization of microtubules is the kinase DCLK1 [95-97]. DCLK1 showed downregulation of phosphorylation on S308 in the P12,000 fraction upon stimulation. The protein SHOT1 (also named SHTN1 or KIAA1598), which is also involved in axon outgrowth by interaction with the actin cytoskeleton in a phosphorylation-dependent manner [98, 99], showed upregulation of S628 phosphorylation in both the P5,000 and P12,000 fractions. The microtubule associated kinase MARK4, which is active in regulation of microtubule dynamics in axons [100] showed upregulation of phosphorylation on S464 in both P5,000 and P12,000. The protein, MARCKS, also involved in axonogenesis and known to be regulated by phosphorylation [101-103], showed upregulation of phosphorylation on S322 in both fractions and downregulation on the sites T143, S145 and T150 in the P5,000 fraction. MARCKS phosphorylation by PKC isoforms has furthermore been associated with induction of neurotransmitter release [104, 105]. The MARCKS related protein MARCKSL1, which influences actin stability and neuronal migration and is known to be regulated by phosphorylation [106], showed upregulation of phosphorylation on a number of sites in both P5,000 and P12,000 after the stimulation (**fig. 7A-B**). MARCKS and MARCKSL1 can bind to Calmodulin, activated by Ca^{2+}, in a PKC regulated way [107-109]. The PKC type epsilon (PRKCE) was also found with regulated phosphosites in both fractions. Changes in phosphorylation of MARCKS and MARCKSL1 were also observed after depolarization of adult rat synaptosomes in a study by Silbern et al. in 2021 [50].

Changes in protein phosphorylation of kinases, ion channels and proteins related to Ca^{2+} signaling

The rise in extracellular KCl is expected to induce depolarization of the membrane leading to Ca^{2+} influx [110]. This then causes activation of e.g. the Ca^{2+} binding protein Calmodulin, which then further activates Calmodulin binding proteins. Much of the intracellular signaling upon depolarization rely on kinase activity and is influenced by ion channel activity [111, 112]. In the

group of proteins with regulation of phosphorylation from the day 90 ALI-CO fractions, 8 are annotated as Calmodulin binding in the P12,000 fraction and 4 of them were also found with regulations in P5,000 (**fig. 7A-B**). These include the MARCKS and MARCKSL1 together with CAMK2 type gamma (CAMK2G), (only in P12,000), an isoform of CAMK2 which is known as a key regulator of synaptic signaling upon membrane depolarization and activated by calmodulin [112-114]. Another calmodulin-binding protein showing significant regulation in phosphorylation is CASK, which plays an important role in neuronal development [115] and affects synaptic function [116, 117]. In the P12,000 fraction, 7 kinases showed changes in phosphorylation including CAMK2G, CASK, MARK4, DCLK1 and PRKCE, and 4 of the kinases also showed regulation in the P5,000 fraction. Three ion channels with significant changes in phosphorylation are found in the P12,000 fraction. One of those is the CACNB1, which is the regulatory B1 subunit of voltage-dependent L-type Ca^{2+} channels [118]. The other two ion channels are PANX1, which may be involved in regulating Ca^{2+} homeostasis [119] and MCOLN1 which is a Ca^{2+} channel involved in Ca^{2+} release from endosomes and lysosomes [120, 121].

Proteins related to synaptogenesis and synaptic transmission show regulation of phosphorylation

Several proteins that are associated with synaptic transmission, synaptic plasticity or synaptic development were among the proteins with changing phosphosites. One such protein was PRKCE, which has been implicated in both neurite outgrowth [122], synaptogenesis [123], strengthening of synaptic connections [124] and synaptic transmission through interaction with the actin cytoskeleton [125]. PRKCE showed upregulation of S346 and S350 phosphorylation in both the P12,000 and P5,000 fractions upon KCl stimulation. S346 and S350 sites are important for activation of PRKCE in the cytoskeleton-related process cytokinesis [126]. CAMK2G showed upregulation of S381 and S384 phosphorylation in the P12,000 fraction. The CAMK2 protein family are well-established actors in synaptic transmission [112-114]. Furthermore, the CAMK2G and epsilon isoforms are the main CAMK2 isoforms expressed during early neurodevelopment [127] and CAMK2G has been shown to influence neuronal maturation [128]. Furthermore, CAMK2 is involved in Ca^{2+}-dependent growth cone motility and axonal growth [129, 130]. The AZ protein RIMS2, which is known to be involved in synaptic vesicle priming [131] showed downregulation of phosphorylation in P12,000. SHANK1, a PSD scaffold protein important for synaptogenesis and establishment of the PSD during synaptic maturation [132], showed upregulation of phosphorylation in both P5,000 and P12,000. Other postsynaptic scaffold proteins that show changes in phosphorylation are DLGAP4 (in both fractions) and DLGAP1 in P12,000. The DLGAP1-4 (also named SAPAP1-4) proteins function together with PSD95 (also named DLG4) and SHANK proteins at the PSD and influence synaptic strength (reviewed in [133]). Furthermore, DLGAP proteins have been shown to influence PSD size, synaptic transmission and social behavior [134-137]. The F-actin binding protein DBN1 (also named ABP1), showed downregulation of S601 phosphorylation in the P5,000 fraction. DBN1 regulates the formation of presynaptic boutons and dendritic spines [138, 139] and interacts with proteins at the PSD and presynaptic AZ [140, 141].

None of the more classical synaptic transmission-related proteins BSN, PCLO, DNM1 or SYN1-3, were found to have significantly regulated phosphosites after stimulation of the day 90 ALI-CO fractions.

Day 150 ALI-CO differential centrifugation fractions show more mature phosphorylation profile after KCl stimulation

The 15s high KCl stimulation was conducted on the P5,000 and P12,000 differential centrifugation fractions from day 150 ALI-COs, again in three technical replicates of the stimulation. The phosphopeptides from stimulated and control samples were enriched and analyzed with LC-MSMS using TMT-labeling for quantification.

The phosphoproteomic analysis identified 6,352 phosphopeptides from 2,592 proteins. Due to high variation between the 3 replicates, which is normal when studying highly dynamic phosphosite changes after short-time stimulations, only a few regulations were detected as significant with PolyStest FDR below 0.05 (P5,000: 13 peptides; P12,000: 4 peptides). Changing the criteria for significance by raising the FDR-value cutoff to 0.2 and FC threshold to ≥ 1.3 up or down, rendered 30 phosphopeptides from 28 proteins in the P5,000 fraction. Due to the high variation, the Limma FDR statistic with Benjamini-Hochberg correction was selected for the P12,000 fraction. Limma FDR was chosen because it uses empirical Bayes moderation to stabilize variance estimates, making it especially suitable for datasets with substantial variability. With these statistics and the same criteria for significance (FDR < 0.2 and FC ≥ 1.3) as for the P5,000 data, the 15s KCl stimulation of the day 150 ALI-CO P12,000 fractions yielded 107 phosphopeptides from 102 proteins within the FDR and FC thresholds.

PPI STRING networks of proteins with the potentially regulated phosphosites from each fraction are shown in **fig. 8A** and **S5** and their sites are indicated (confidence score cutoff: 0.4, only connected nodes are shown). The P5,000 fraction proteins showed GO CC and Molecular function (MF) enrichment in several cytoskeleton related terms, e.g. Cytoskeleton (FDR: 0.0089, 15 proteins), Microtubule (FDR: 0.0269, 7 proteins) and Cytoskeletal protein binding (FDR: 0.036, 11 proteins). Some key synaptic proteins involved in synaptic transmission showed potential differential regulation in phosphorylation, such as DNM1 showing the downregulation in S774 phosphorylation which, as earlier mentioned, is characteristic for stimulation-dependent endocytosis as part of the synaptic vesicle cycle. Other synaptic proteins with potential regulations were the proteins PCLO, SYN1, SYNJ1 and MAP1B (**fig. 8A**).

The P12,000 fraction proteins with potential regulations in phosphorylation showed GO CC and MF enrichment of terms such as Neuron projection (FDR: 0.0017, 31 proteins), Synapse (FDR: 0.0018, 32 proteins), Cytoskeleton (FDR: 0.0025, 35 proteins), Cell junction (FDR: 0.0039, 39 proteins) and Calmodulin binding (FDR: 0.0027, 11 proteins) (**fig. 8C-D**). A PPI of the proteins belonging to the GO CC term synapse is shown in **fig. 8B** (confidence score cutoff: 0.7, connected nodes only). These included e.g. SLC17A7 (Vesicular glutamate transporter 1 or VGLUT1), MAPT, SYN1, MAP2, BSN and

PTEN. Furthermore, phosphosites were potentially regulated in the calmodulin-regulated kinase CAMK2G, a key regulator of synaptic transmission, as earlier mentioned [112-114]. Additionally, the growth cone marker GAP43 showed potential regulation in phosphorylation (**fig. 8B**).

Overall, the stimulation of ALI-CO day 150 fractions P5,000 and P12,000 resulted in potential differential regulation of classical synaptic transmission proteins such as DNM1, SYN1, PCLO, CAMK2G and BSN indicating a more mature phosphorylation profile compared to the earlier timepoint, day 90.

Discussion

Here we have used a variation of differential centrifugation to design a method for enrichment of synaptosomes and synaptic proteins from human NOs. The method shows high reproducibility between different brain tissues and NO types and provides a simpler strategy for enrichment than the classical density gradient-based methods. The method performs well with low amounts of tissue, which is desirable when working e.g. with human brain and NO samples.

The differential centrifugation workflow presented here showed significant and consistent enrichment of synaptosomes/synaptic structures and synaptic proteins from several neural or brain tissue types – mouse brain at two developmental stages (newborn and adult), adult human cortex and two NO types, FBOs and ALI-COs. The P5,000 and P12,000 fractions from adult mouse and human brain tissue clearly contained membrane enclosed synaptosomes with mitochondria and synaptic vesicles, frequently with PSD attached. Generally, the enrichment level of synaptic proteins was comparable to a standard Percoll density gradient enrichment procedure. Furthermore, the differential centrifugation workflow resulted in significant enrichment of growth cones in the form of GCPs from the day 90 ALI-COs as indicated by both protein markers and TEM images. The GPCs were comparable to GPCs isolated with synaptosome enrichment protocols in other studies presenting with fibrous content, larger vesicles and mitochondria [82-84]. At the more mature stage, day 150 ALI-COs, the differential centrifugation resulted in enrichment of immature synaptosomes with the presence of synaptic vesicles and mitochondria. The ALI-CO organoid type seemed the most material-efficient organoid model to use, which is particularly important when studying protein phosphorylation. We speculate that the reason for this observation might be that the ALI-CO method significantly reduces the necrotic core compared to culture of spherical organoids [71]. However, the difference in protein yield between FBOs and ALI-COs did not show statistical significance with the limited number of replicates used.

The mitochondrial content was significantly higher in the P5,000 compared to the other fractions across tissue types, while the P22,000 fractions contained mainly membrane material as documented by protein enrichment and TEM images. These findings are consistent with those reported in other studies on subcellular fractionation, which observed pelleting of mitochondria around 3,000xg and endosome and Golgi apparatus proteins around 12,000-24,000xg [67, 69]. Considering the high level of mitochondrial content in the P5,000 fraction, the P12,000 fraction seems to contain the purest enrichment of synaptosomes/GCPs from the organoid tissues. This could also explain why we can observe more stimulation-induced changes in the phosphorylation profile from this fraction from the organoids as high non-synaptic mitochondrial contamination will obscure the detection of phosphopeptides. Although the P22,000 fraction also showed significant enrichment in synaptic proteins, especially postsynaptic membrane proteins from the young tissues, the TEM showed none or very few synaptosomes or GCPs in this fraction. This suggests that functional synaptosomes are not preserved in P22,000.

The P5,000 fraction from mouse brain showed depolarization-dependent changes in phosphorylation of key synaptic proteins when stimulated with KCl, similar to what has been observed in previously published characterizations of activated synaptosomes [49-51]. This included changes in phosphorylation of proteins that are important components at the AZ or in the synaptic vesicle cycle such as PCLO, BSN, ERC2, SYN1 and DNM1. The P12,000 adult mouse fraction showed smaller changes in phosphorylation upon stimulation, whereas the P22,000 did not seem to respond, likely because most functional synaptosomes have been pelleted in the previous fractions. In mature brain tissue, the synaptosomes have higher density than those from the younger tissue types [83], and thus likely end up more frequently in the P5,000 fraction where we also see larger non-synaptic mitochondrial contamination. This is likely the explanation why we observe most changes in the P5,000 fraction, while the number of regulated phosphopeptides is small compared to other studies [49, 51] likely due to the mitochondrial contamination. However, the overall results indicate that synaptosomes enriched with the differential centrifugation method described here are viable and can be used to study stimulation-dependent changes in phosphorylation.

The stimulation of day 90 ALI-CO P5,000 and P12,000 fractions resulted in significant changes in protein phosphorylation, which was replicated between the fractions. More changes in phosphorylation sites were observed in the P12,000 fraction, which could be due to mitochondrial contamination in P5,000, interfering with the analysis and perhaps due to a higher yield of synaptic structures and GCPs in P12,000 as a consequence of their lower density in this young tissue. The stimulation-induced changes in phosphorylation of proteins related to Ca^{2+} signaling, Ca^{2+} ion flux and kinase activity indicated that the KCl stimulation caused depolarization of the GCPs in the fractions. It is known that growth cones contain voltage-gated Ca^{2+} channels, and that depolarization with patch-clamp methods or high KCl stimulation causes influx of Ca^{2+} ions [142]. Several studies have shown stimulation-induced depolarization of both intact [142-149] and isolated GCPs [143, 144, 148, 150, 151] similar to the high KCl stimulation in the present study. Growth cones are affected by various external molecules in the process of axon guidance and synaptogenesis, many of which have been shown to alter intracellular Ca^{2+} levels (reviewed in [152] and [153]). It is well-established that a balance in intracellular Ca^{2+} levels is key to growth cone motility, as moderate levels will increase outgrowth and can promote turning of growth cones, whereas higher levels cause retraction and disruption of microfilaments [154] [142]. Cytoskeletal processes are generally known to be important in growth cone dynamics, motility and synaptogenesis [155-157]. Thus, a depolarization of the GCPs structures from day 90 ALI-COs most likely caused changes in cytoskeletal processes as indicated by the present results. However, many of the detected phosphosites with significant changes were either not known, or their functions have not been examined, which is a frequent challenge in MS-based studies of protein phosphorylation. Furthermore, since protein phosphorylation can both lead to activation and deactivation of proteins as well as generation of new interaction sites, it was not possible to determine specifically which processes the stimulation initiated. Though several proteins involved in synaptic transmission was enriched in the fractions, they did show significant differential regulation

of phosphorylation upon stimulation. This is likely due to the early developmental stage and furthermore, a potential regulation in some synaptosomes present in the fractions, could be masked by the higher amount of GCPs.

High KCl stimulation of the day 150 ALI-CO P5,000 and P12,000 fractions showed, despite high variation in the data, a clear tendency of a more mature phosphorylation profile compared to day 90, including changes in proteins that are important players in synaptic transmission and known to be activated by changes in phosphorylation. Though some studies have shown electrical activity in NOs at relatively early time points [59, 65], NOs generally seem to develop network activity from around 3-4 months and forward [65, 158]. This indicates a larger number of functional synapses present at later timepoints, which is in line with our findings here. Thus, day 90 seems too early for studying classical synaptic transmission, whereas at later stages of differentiation enables the study of the classical synaptic transmission mechanisms using human NO tissue.

The stimulation of the ALI-CO fractions showed phosphorylation changes in numerous proteins related to brain development, synaptogenesis, and axonal growth. Many of these proteins have been implicated in neurodevelopmental disorders such as autism spectrum disorders (SHANK1 (reviewed in [159]), DLGAP4 [137] and MAP1B [160, 161]), intellectual disability (MAP1B [160, 162], CAMK2G [128], DLGAP4 [137] and CASK [163, 164]) and schizophrenia (DCLK1 [165, 166], MARCKS [167, 168], PRKCE [169] and SHANK1 [170, 171]). Thus, the enrichment of immature synapses/GCPs from NOs could be used to study early disease related changes in protein expression and the changes in stimulation-induced protein activity related to neurodevelopmental disorders using various kinds of stimulations.

The differential centrifugation method described here offers a simple protocol for enrichment of synaptic proteins from NOs without the need for density gradients, and which can be performed within a short time. This could be used to study the development of function and disease-related changes in human synapses in organoid tissue, which is easy to access and manipulate. The yield of sample material is relatively high compared to the density gradient enrichments, which can be demanding and expensive to achieve when working with organoids. Though the classical density gradient enrichment methods likely generate a purer enrichment when working with rodent or human brain tissue, the density gradient methods do not work as efficiently as the differential centrifugation method when using NO tissue, perhaps due to lower number of synapses in the NO tissue compared to adult brain tissues and a lower density in younger synapses. Using the presented method, we showed enrichment of synaptosomes from adult human and mouse brain tissue and were furthermore able to successfully conduct and examine protein phosphorylation changes caused by stimulation-induced depolarization of adult mouse synaptosomes, GCPs and immature synaptosomes isolated from ALI-COs. Thus, the method could be used to study intracellular signaling in growth cones caused by external stimulation with axon guidance molecules and changes in these processes related to neurodevelopmental diseases. Furthermore, with the option of extended culture of neural organoids for up to several years, it will be possible to study

these processes over time and follow the synaptic development from growth cones into mature synapses.

Acknowledgements

The present project was primarily funded by the Independent Research Fund Denmark in the category of Natural Science (project no. 95-31003-2323588). Parts of the project were funded by the Lundbeck Foundation under the DEVELOPNOID project (no. 95-31003-3373400). Immunofluorescent image acquisition was conducted at the Danish Molecular Biomedical Imaging Center (DaMBIC, University of Southern Denmark), supported by the Novo Nordisk Foundation (NNF) (grant agreement no. NNF18SA0032928).

References

1. Bayés, A., et al., *Characterization of the proteome, diseases and evolution of the human postsynaptic density.* Nat Neurosci, 2011. **14**(1): p. 19-21.
2. Masini, E., et al., *An Overview of the Main Genetic, Epigenetic and Environmental Factors Involved in Autism Spectrum Disorder Focusing on Synaptic Activity.* Int J Mol Sci, 2020. **21**(21).
3. Trobiani, L., et al., *The neuroligins and the synaptic pathway in Autism Spectrum Disorder.* Neurosci Biobehav Rev, 2020. **119**: p. 37-51.
4. Howes, O.D. and E. Shatalina, *Integrating the Neurodevelopmental and Dopamine Hypotheses of Schizophrenia and the Role of Cortical Excitation-Inhibition Balance.* Biol Psychiatry, 2022. **92**(6): p. 501-513.
5. Legge, S.E., et al., *Genetic architecture of schizophrenia: a review of major advancements.* Psychol Med, 2021. **51**(13): p. 2168-2177.
6. Fukata, Y. and M. Fukata, *Epilepsy and synaptic proteins.* Curr Opin Neurobiol, 2017. **45**: p. 1-8.
7. Naseri, N.N., et al., *The complexity of tau in Alzheimer's disease.* Neurosci Lett, 2019. **705**: p. 183-194.
8. Wang, R. and P.H. Reddy, *Role of Glutamate and NMDA Receptors in Alzheimer's Disease.* J Alzheimers Dis, 2017. **57**(4): p. 1041-1048.
9. Nguyen, M., et al., *Synaptic, Mitochondrial, and Lysosomal Dysfunction in Parkinson's Disease.* Trends Neurosci, 2019. **42**(2): p. 140-149.
10. Henderson, M.X., J.Q. Trojanowski, and V.M. Lee, *α-Synuclein pathology in Parkinson's disease and related α-synucleinopathies.* Neurosci Lett, 2019. **709**: p. 134316.
11. Whittaker, V.P., *The isolation and characterization of acetylcholine-containing particles from brain.* The Biochemical journal, 1959. **72**(4): p. 694-706.
12. Hebb, C.O. and V.P. Whittaker, *Intracellular distributions of acetylcholine and choline acetylase.* The Journal of Physiology, 1958. **142**(1): p. 187-196.
13. Bradford, H.F., *Metabolic response of synaptosomes to electrical stimulation: release of amino acids.* Brain Res, 1970. **19**(2): p. 239-47.
14. De Belleroche, J.S. and H.F. Bradford, *Metabolism of beds of mammalian cortical synaptosomes: response to depolarizing influences.* J Neurochem, 1972. **19**(3): p. 585-602.
15. Booth, R.F. and J.B. Clark, *A rapid method for the preparation of relatively pure metabolically competent synaptosomes from rat brain.* Biochem J, 1978. **176**(2): p. 365-70.
16. Nicholls, D.G. and T.S. Sihra, *Synaptosomes possess an exocytotic pool of glutamate.* Nature, 1986. **321**(6072): p. 772-773.
17. Whittaker, V.P., *The isolation and characterization of acetylcholine-containing particles from brain.* Biochem J, 1959. **72**: p. 694-706.
18. Dunkley, P.R., et al., *A rapid method for isolation of synaptosomes on Percoll gradients.* Brain Res, 1986. **372**(1): p. 115-29.
19. Dunkley, P.R., P.E. Jarvie, and P.J. Robinson, *A rapid Percoll gradient procedure for preparation of synaptosomes.* Nat Protoc, 2008. **3**(11): p. 1718-28.
20. Ling, C.M. and A.A. Abdel-Latif, *Studies on sodium transport in rat brain nerve-ending particles.* J Neurochem, 1968. **15**(8): p. 721-9.
21. Evans, G.J., *The synaptosome as a model system for studying synaptic physiology.* Cold Spring Harb Protoc, 2015. **2015**(5): p. 421-4.
22. Koopmans, F., et al., *SynGO: An Evidence-Based, Expert-Curated Knowledge Base for the Synapse.* Neuron, 2019. **103**(2): p. 217-234.e4.
23. Pappireddi, N., L. Martin, and M. Wühr, *A Review on Quantitative Multiplexed Proteomics.* Chembiochem, 2019. **20**(10): p. 1210-1224.
24. Rozanova, S., et al., *Quantitative Mass Spectrometry-Based Proteomics: An Overview.* Methods Mol Biol, 2021. **2228**: p. 85-116.
25. Leutert, M., S.W. Entwisle, and J. Villén, *Decoding Post-Translational Modification Crosstalk With Proteomics.* Mol Cell Proteomics, 2021. **20**: p. 100129.
26. Larsen, M.R., et al., *Exploring the sialiome using titanium dioxide chromatography and mass spectrometry.* Mol Cell Proteomics, 2007. **6**(10): p. 1778-87.
27. Melo-Braga, M.N., et al., *Comprehensive protocol to simultaneously study protein phosphorylation, acetylation, and N-linked sialylated glycosylation.* Methods Mol Biol, 2015. **1295**: p. 275-92.

28. Melo-Braga, M.N., et al., *Comprehensive quantitative comparison of the membrane proteome, phosphoproteome, and sialiome of human embryonic and neural stem cells.* Mol Cell Proteomics, 2014. **13**(1): p. 311-28.
29. Palmisano, G., et al., *A novel method for the simultaneous enrichment, identification, and quantification of phosphopeptides and sialylated glycopeptides applied to a temporal profile of mouse brain development.* Mol Cell Proteomics, 2012. **11**(11): p. 1191-202.
30. Kang, T., et al., *Characterization of the Molecular Mechanisms Underlying Glucose Stimulated Insulin Secretion from Isolated Pancreatic β-cells Using Post-translational Modification Specific Proteomics (PTMomics).* Mol Cell Proteomics, 2018. **17**(1): p. 95-110.
31. Boll, I., et al., *Depolarization-dependent Induction of Site-specific Changes in Sialylation on N-linked Glycoproteins in Rat Nerve Terminals.* Mol Cell Proteomics, 2020. **19**(9): p. 1418-1435.
32. Chang, R.Y., et al., *The synaptic proteome in Alzheimer's disease.* Alzheimers Dement, 2013. **9**(5): p. 499-511.
33. Chang, R.Y., et al., *Targeted quantitative analysis of synaptic proteins in Alzheimer's disease brain.* Neurochem Int, 2014. **75**: p. 66-75.
34. Chang, R.Y., et al., *SWATH analysis of the synaptic proteome in Alzheimer's disease.* Neurochem Int, 2015. **87**: p. 1-12.
35. Gyorffy, B.A., et al., *Synaptic mitochondrial dysfunction and septin accumulation are linked to complement-mediated synapse loss in an Alzheimer's disease animal model.* Cell Mol Life Sci, 2020. **77**(24): p. 5243-5258.
36. Shen, L., et al., *Proteomic Profiling of Cerebrum Mitochondria, Myelin Sheath, and Synaptosome Revealed Mitochondrial Damage and Synaptic Impairments in Association with 3 x Tg-AD Mice Model.* Cell Mol Neurobiol, 2022. **42**(6): p. 1745-1763.
37. Shi, L., et al., *Cumulative effects of the ApoE genotype and gender on the synaptic proteome and oxidative stress in the mouse brain.* Int J Neuropsychopharmacol, 2014. **17**(11): p. 1863-79.
38. Zeppillo, T., et al., *Functional impairment of cortical AMPA receptors in schizophrenia.* Schizophr Res, 2022. **249**: p. 25-37.
39. Zhou, K., et al., *NMDA receptor hypofunction induces dysfunctions of energy metabolism and semaphorin signaling in rats: a synaptic proteome study.* Schizophr Bull, 2012. **38**(3): p. 579-91.
40. Bonneau, M., et al., *Functional brain defects in a mouse model of a chromosomal t(1;11) translocation that disrupts DISC1 and confers increased risk of psychiatric illness.* Transl Psychiatry, 2021. **11**(1): p. 135.
41. Paternoster, V., et al., *Brain proteome changes in female Brd1(+/-) mice unmask dendritic spine pathology and show enrichment for schizophrenia risk.* Neurobiol Dis, 2019. **124**: p. 479-488.
42. Ramos-Miguel, A., et al., *The SNAP25 Interactome in Ventromedial Caudate in Schizophrenia Includes the Mitochondrial Protein ARF1.* Neuroscience, 2019. **420**: p. 97-111.
43. Corena-McLeod, M., et al., *New model of action for mood stabilizers: phosphoproteome from rat pre-frontal cortex synaptoneurosomal preparations.* PLoS One, 2013. **8**(5): p. e52147.
44. Plum, S., et al., *Proteomic Characterization of Synaptosomes from Human Substantia Nigra Indicates Altered Mitochondrial Translation in Parkinson's Disease.* Cells, 2020. **9**(12).
45. Almikhlafi, M.A., et al., *Deletion of DJ-1 in rats affects protein abundance and mitochondrial function at the synapse.* Sci Rep, 2020. **10**(1): p. 13719.
46. Betzer, C., et al., *Identification of synaptosomal proteins binding to monomeric and oligomeric alpha-synuclein.* PLoS One, 2015. **10**(2): p. e0116473.
47. Blumenstock, S., et al., *Early defects in translation elongation factor 1alpha levels at excitatory synapses in alpha-synucleinopathy.* Acta Neuropathol, 2019. **138**(6): p. 971-986.
48. Szego, E.M., et al., *Cytosolic Trapping of a Mitochondrial Heat Shock Protein Is an Early Pathological Event in Synucleinopathies.* Cell Rep, 2019. **28**(1): p. 65-77 e6.
49. Engholm-Keller, K., et al., *The temporal profile of activity-dependent presynaptic phospho-signalling reveals long-lasting patterns of poststimulus regulation.* PLoS Biol, 2019. **17**(3): p. e3000170.
50. Silbern, I., et al., *Protein Phosphorylation in Depolarized Synaptosomes: Dissecting Primary Effects of Calcium from Synaptic Vesicle Cycling.* Mol Cell Proteomics, 2021. **20**: p. 100061.
51. Kohansal-Nodehi, M., et al., *Analysis of protein phosphorylation in nerve terminal reveals extensive changes in active zone proteins upon exocytosis.* Elife, 2016. **5**.
52. McGonigle, P. and B. Ruggeri, *Animal models of human disease: Challenges in enabling translation.* Biochemical Pharmacology, 2014. **87**(1): p. 162-171.
53. Renner, M., et al., *Self-organized developmental patterning and differentiation in cerebral organoids.* Embo j, 2017. **36**(10): p. 1316-1329.

54. Qian, X., et al., *Brain-Region-Specific Organoids Using Mini-bioreactors for Modeling ZIKV Exposure.* Cell, 2016. **165**(5): p. 1238-1254.
55. Camp, J.G., et al., *Human cerebral organoids recapitulate gene expression programs of fetal neocortex development.* Proc Natl Acad Sci U S A, 2015. **112**(51): p. 15672-7.
56. Amiri, A., et al., *Transcriptome and epigenome landscape of human cortical development modeled in organoids.* Science, 2018. **362**(6420).
57. Paşca, A.M., et al., *Functional cortical neurons and astrocytes from human pluripotent stem cells in 3D culture.* Nat Methods, 2015. **12**(7): p. 671-8.
58. Lancaster, M.A., et al., *Cerebral organoids model human brain development and microcephaly.* Nature, 2013. **501**(7467): p. 373-9.
59. Mariani, J., et al., *FOXG1-Dependent Dysregulation of GABA/Glutamate Neuron Differentiation in Autism Spectrum Disorders.* Cell, 2015. **162**(2): p. 375-390.
60. Yakoub, A.M., *Cerebral organoids exhibit mature neurons and astrocytes and recapitulate electrophysiological activity of the human brain.* Neural Regen Res, 2019. **14**(5): p. 757-761.
61. Yakoub, A.M. and M. Sadek, *Analysis of Synapses in Cerebral Organoids.* Cell Transplant, 2019. **28**(9-10): p. 1173-1182.
62. Passaro, A.P. and S.L. Stice, *Electrophysiological Analysis of Brain Organoids: Current Approaches and Advancements.* Front Neurosci, 2020. **14**: p. 622137.
63. Logan, S., et al., *Dynamic Characterization of Structural, Molecular, and Electrophysiological Phenotypes of Human-Induced Pluripotent Stem Cell-Derived Cerebral Organoids, and Comparison with Fetal and Adult Gene Profiles.* Cells, 2020. **9**(5).
64. Quadrato, G., et al., *Cell diversity and network dynamics in photosensitive human brain organoids.* Nature, 2017. **545**(7652): p. 48-53.
65. Fair, S.R., et al., *Electrophysiological Maturation of Cerebral Organoids Correlates with Dynamic Morphological and Cellular Development.* Stem Cell Reports, 2020. **15**(4): p. 855-868.
66. Giandomenico, S.L., M. Sutcliffe, and M.A. Lancaster, *Generation and long-term culture of advanced cerebral organoids for studying later stages of neural development.* Nat Protoc, 2021. **16**(2): p. 579-602.
67. Geladaki, A., et al., *Combining LOPIT with differential ultracentrifugation for high-resolution spatial proteomics.* Nat Commun, 2019. **10**(1): p. 331.
68. Itzhak, D.N., et al., *A Mass Spectrometry-Based Approach for Mapping Protein Subcellular Localization Reveals the Spatial Proteome of Mouse Primary Neurons.* Cell Rep, 2017. **20**(11): p. 2706-2718.
69. Itzhak, D.N., et al., *Global, quantitative and dynamic mapping of protein subcellular localization.* Elife, 2016. **5**.
70. Sloan, S.A., et al., *Generation and assembly of human brain region-specific three-dimensional cultures.* Nat Protoc, 2018. **13**(9): p. 2062-2085.
71. Giandomenico, S.L., et al., *Cerebral organoids at the air-liquid interface generate diverse nerve tracts with functional output.* Nat Neurosci, 2019. **22**(4): p. 669-679.
72. Heissel, S., et al., *Evaluation of spectral libraries and sample preparation for DIA-LC-MS analysis of host cell proteins: A case study of a bacterially expressed recombinant biopharmaceutical protein.* Protein Expr Purif, 2018. **147**: p. 69-77.
73. Thingholm, T.E., et al., *Highly selective enrichment of phosphorylated peptides using titanium dioxide.* Nat Protoc, 2006. **1**(4): p. 1929-35.
74. Larsen, M.R., et al., *Highly selective enrichment of phosphorylated peptides from peptide mixtures using titanium dioxide microcolumns.* Mol Cell Proteomics, 2005. **4**(7): p. 873-86.
75. Ting, L., et al., *MS3 eliminates ratio distortion in isobaric multiplexed quantitative proteomics.* Nat Methods, 2011. **8**(11): p. 937-40.
76. Schwämmle, V., et al., *PolySTest: Robust Statistical Testing of Proteomics Data with Missing Values Improves Detection of Biologically Relevant Features.* Mol Cell Proteomics, 2020. **19**(8): p. 1396-1408.
77. Doncheva, N.T., et al., *Cytoscape StringApp: Network Analysis and Visualization of Proteomics Data.* Journal of Proteome Research, 2019. **18**(2): p. 623-632.
78. Legeay, M., et al., *Visualize omics data on networks with Omics Visualizer, a Cytoscape App.* F1000Res, 2020. **9**: p. 157.
79. R Core Team, R., *R: A language and environment for statistical computing.* 2013.
80. Wilkinson, L., *ggplot2: Elegant Graphics for Data Analysis by WICKHAM, H.* Biometrics, 2011. **67**(2): p. 678-679.
81. Kolde, R., *pheatmap: Pretty Heatmaps.* 2019.

82. Pfenninger, K.H., et al., *Nerve growth cones isolated from fetal rat brain: subcellular fractionation and characterization.* Cell, 1983. **35**(2 Pt 1): p. 573-84.
83. Grove, W.E., et al., *Qualitative and quantitative morphological changes in subcellular fractions from mouse cerebral cortex during postnatal development.* J Cell Biol, 1973. **58**(3): p. 676-88.
84. Gordon-Weeks, P.R. and R.O. Lockerbie, *Isolation and partial characterisation of neuronal growth cones from neonatal rat forebrain.* Neuroscience, 1984. **13**(1): p. 119-36.
85. Nozumi, M., et al., *Identification of functional marker proteins in the mammalian growth cone.* Proc Natl Acad Sci U S A, 2009. **106**(40): p. 17211-6.
86. Estrada-Bernal, A., et al., *Functional complexity of the axonal growth cone: a proteomic analysis.* PLoS One, 2012. **7**(2): p. e31858.
87. Fishman, M.C., *GAP-43: putting constraints on neuronal plasticity.* Perspect Dev Neurobiol, 1996. **4**(2-3): p. 193-8.
88. Mozhayeva, M.G., et al., *Development of vesicle pools during maturation of hippocampal synapses.* J Neurosci, 2002. **22**(3): p. 654-65.
89. Ashrafian, S., et al., *Quantitative Phosphoproteomics and Acetylomics of Safranal Anticancer Effects in Triple-Negative Breast Cancer Cells.* J Proteome Res, 2022. **21**(11): p. 2566-2585.
90. Xue, J., et al., *Calcineurin selectively docks with the dynamin Ixb splice variant to regulate activity-dependent bulk endocytosis.* J Biol Chem, 2011. **286**(35): p. 30295-30303.
91. Gordon-Weeks, P.R. and I. Fischer, *MAP1B expression and microtubule stability in growing and regenerating axons.* Microsc Res Tech, 2000. **48**(2): p. 63-74.
92. Meixner, A., et al., *MAP1B is required for axon guidance and Is involved in the development of the central and peripheral nervous system.* J Cell Biol, 2000. **151**(6): p. 1169-78.
93. Tymanskyj, S.R., T.M. Scales, and P.R. Gordon-Weeks, *MAP1B enhances microtubule assembly rates and axon extension rates in developing neurons.* Mol Cell Neurosci, 2012. **49**(2): p. 110-9.
94. Brugg, B., D. Reddy, and A. Matus, *Attenuation of microtubule-associated protein 1B expression by antisense oligodeoxynucleotides inhibits initiation of neurite outgrowth.* Neuroscience, 1993. **52**(3): p. 489-96.
95. Lin, P.T., et al., *DCAMKL1 encodes a protein kinase with homology to doublecortin that regulates microtubule polymerization.* J Neurosci, 2000. **20**(24): p. 9152-61.
96. Deuel, T.A., et al., *Genetic interactions between doublecortin and doublecortin-like kinase in neuronal migration and axon outgrowth.* Neuron, 2006. **49**(1): p. 41-53.
97. Bergoglio, E., et al., *Spatial and temporal diversity of DCLK1 isoforms in developing mouse brain.* Neurosci Res, 2021. **170**: p. 154-165.
98. Shimada, T., et al., *Shootin1 interacts with actin retrograde flow and L1-CAM to promote axon outgrowth.* J Cell Biol, 2008. **181**(5): p. 817-29.
99. Toriyama, M., et al., *Conversion of a signal into forces for axon outgrowth through Pak1-mediated shootin1 phosphorylation.* Curr Biol, 2013. **23**(6): p. 529-34.
100. Trinczek, B., et al., *MARK4 is a novel microtubule-associated proteins/microtubule affinity-regulating kinase that binds to the cellular microtubule network and to centrosomes.* J Biol Chem, 2004. **279**(7): p. 5915-23.
101. Xu, X.H., et al., *MARCKS regulates membrane targeting of Rab10 vesicles to promote axon development.* Cell Res, 2014. **24**(5): p. 576-94.
102. Brudvig, J.J., et al., *MARCKS regulates neuritogenesis and interacts with a CDC42 signaling network.* Sci Rep, 2018. **8**(1): p. 13278.
103. Tanabe, A., et al., *MARCKS dephosphorylation is involved in bradykinin-induced neurite outgrowth in neuroblastoma SH-SY5Y cells.* J Cell Physiol, 2012. **227**(2): p. 618-29.
104. Li, J., et al., *Myristoylated alanine-rich C kinase substrate-mediated neurotensin release via protein kinase C-delta downstream of the Rho/ROK pathway.* J Biol Chem, 2005. **280**(9): p. 8351-7.
105. Goodall, A.R., et al., *Activation of protein kinase C-alpha and translocation of the myristoylated alanine-rich C-kinase substrate correlate with phorbol ester-enhanced noradrenaline release from SH-SY5Y human neuroblastoma cells.* J Neurochem, 1997. **68**(1): p. 392-401.
106. Björkblom, B., et al., *c-Jun N-terminal kinase phosphorylation of MARCKSL1 determines actin stability and migration in neurons and in cancer cells.* Mol Cell Biol, 2012. **32**(17): p. 3513-26.
107. Porumb, T., et al., *Calcium binding and conformational properties of calmodulin complexed with peptides derived from myristoylated alanine-rich C kinase substrate (MARCKS) and MARCKS-related protein (MRP).* Eur Biophys J, 1997. **25**(4): p. 239-47.

108. Verghese, G.M., et al., *Protein kinase C-mediated phosphorylation and calmodulin binding of recombinant myristoylated alanine-rich C kinase substrate (MARCKS) and MARCKS-related protein.* J Biol Chem, 1994. **269**(12): p. 9361-7.
109. Nairn, A.C. and A. Aderem, *Calmodulin and protein kinase C cross-talk: the MARCKS protein is an actin filament and plasma membrane cross-linking protein regulated by protein kinase C phosphorylation and by calmodulin.* Ciba Found Symp, 1992. **164**: p. 145-54; discussion 154-61.
110. Feligioni, M., A. Nishimune, and J.M. Henley, *Protein SUMOylation Modulates Calcium Influx and Glutamate Release From Presynaptic Terminals.* European Journal of Neuroscience, 2009. **29**(7): p. 1348-1356.
111. Zong, P. and L. Yue, *Regulation of Presynaptic Calcium Channels.* Adv Neurobiol, 2023. **33**: p. 171-202.
112. Wang, Z.W., *Regulation of synaptic transmission by presynaptic CaMKII and BK channels.* Mol Neurobiol, 2008. **38**(2): p. 153-66.
113. Takemoto-Kimura, S., et al., *Calmodulin kinases: essential regulators in health and disease.* J Neurochem, 2017. **141**(6): p. 808-818.
114. Yasuda, R., Y. Hayashi, and J.W. Hell, *CaMKII: a central molecular organizer of synaptic plasticity, learning and memory.* Nature Reviews Neuroscience, 2022. **23**(11): p. 666-682.
115. Hsueh, Y.P., *The role of the MAGUK protein CASK in neural development and synaptic function.* Curr Med Chem, 2006. **13**(16): p. 1915-27.
116. Atasoy, D., et al., *Deletion of CASK in mice is lethal and impairs synaptic function.* Proc Natl Acad Sci U S A, 2007. **104**(7): p. 2525-30.
117. McSweeney, D., et al., *CASK loss of function differentially regulates neuronal maturation and synaptic function in human induced cortical excitatory neurons.* iScience, 2022. **25**(10): p. 105187.
118. Cohen, R.M., et al., *Unique modulation of L-type Ca2+ channels by short auxiliary beta1d subunit present in cardiac muscle.* Am J Physiol Heart Circ Physiol, 2005. **288**(5): p. H2363-74.
119. Vanden Abeele, F., et al., *Functional implications of calcium permeability of the channel formed by pannexin 1.* J Cell Biol, 2006. **174**(4): p. 535-46.
120. LaPlante, J.M., et al., *Identification and characterization of the single channel function of human mucolipin-1 implicated in mucolipidosis type IV, a disorder affecting the lysosomal pathway.* FEBS Lett, 2002. **532**(1-2): p. 183-7.
121. LaPlante, J.M., et al., *Functional links between mucolipin-1 and Ca2+-dependent membrane trafficking in mucolipidosis IV.* Biochem Biophys Res Commun, 2004. **322**(4): p. 1384-91.
122. Fagerström, S., et al., *Protein kinase C-epsilon is implicated in neurite outgrowth in differentiating human neuroblastoma cells.* Cell Growth Differ, 1996. **7**(6): p. 775-85.
123. Sen, A., et al., *Protein Kinase Cε (PKCε) Promotes Synaptogenesis through Membrane Accumulation of the Postsynaptic Density Protein PSD-95.* J Biol Chem, 2016. **291**(32): p. 16462-76.
124. Wang, X.T., et al., *cAMP-EPAC-PKCε-RIM1α signaling regulates presynaptic long-term potentiation and motor learning.* Elife, 2023. **12**.
125. Prekeris, R., et al., *Identification and localization of an actin-binding motif that is unique to the epsilon isoform of protein kinase C and participates in the regulation of synaptic function.* J Cell Biol, 1996. **132**(1-2): p. 77-90.
126. Saurin, A.T., et al., *The regulated assembly of a PKCepsilon complex controls the completion of cytokinesis.* Nat Cell Biol, 2008. **10**(8): p. 891-901.
127. Bayer, K.U., et al., *Developmental expression of the CaM kinase II isoforms: ubiquitous gamma- and delta-CaM kinase II are the early isoforms and most abundant in the developing nervous system.* Brain Res Mol Brain Res, 1999. **70**(1): p. 147-54.
128. Proietti Onori, M., et al., *The intellectual disability-associated CAMK2G p.Arg292Pro mutation acts as a pathogenic gain-of-function.* Hum Mutat, 2018. **39**(12): p. 2008-2024.
129. Xi, F., et al., *Calcium/calmodulin-dependent protein kinase II regulates mammalian axon growth by affecting F-actin length in growth cone.* J Cell Physiol, 2019. **234**(12): p. 23053-23065.
130. Wen, Z., et al., *A CaMKII/calcineurin switch controls the direction of Ca(2+)-dependent growth cone guidance.* Neuron, 2004. **43**(6): p. 835-46.
131. Kaeser, P.S., et al., *RIM genes differentially contribute to organizing presynaptic release sites.* Proc Natl Acad Sci U S A, 2012. **109**(29): p. 11830-5.
132. Grabrucker, A.M., et al., *Concerted action of zinc and ProSAP/Shank in synaptogenesis and synapse maturation.* Embo j, 2011. **30**(3): p. 569-81.
133. Rasmussen, A.H., H.B. Rasmussen, and A. Silahtaroglu, *The DLGAP family: neuronal expression, function and role in brain disorders.* Mol Brain, 2017. **10**(1): p. 43.

134. Coba, M.P., et al., *Dlgap1 knockout mice exhibit alterations of the postsynaptic density and selective reductions in sociability.* Sci Rep, 2018. **8**(1): p. 2281.
135. Jiang-Xie, L.F., et al., *Autism-associated gene Dlgap2 mutant mice demonstrate exacerbated aggressive behaviors and orbitofrontal cortex deficits.* Mol Autism, 2014. **5**: p. 32.
136. Welch, J.M., et al., *Cortico-striatal synaptic defects and OCD-like behaviours in Sapap3-mutant mice.* Nature, 2007. **448**(7156): p. 894-900.
137. Schob, C., et al., *Cognitive impairment and autistic-like behaviour in SAPAP4-deficient mice.* Transl Psychiatry, 2019. **9**(1): p. 7.
138. Koch, N., et al., *Terminal axonal arborization and synaptic bouton formation critically rely on abp1 and the arp2/3 complex.* PLoS One, 2014. **9**(5): p. e97692.
139. Haeckel, A., et al., *The actin-binding protein Abp1 controls dendritic spine morphology and is important for spine head and synapse formation.* J Neurosci, 2008. **28**(40): p. 10031-44.
140. Qualmann, B., et al., *Linkage of the actin cytoskeleton to the postsynaptic density via direct interactions of Abp1 with the ProSAP/Shank family.* J Neurosci, 2004. **24**(10): p. 2481-95.
141. Fenster, S.D., et al., *Interactions between Piccolo and the actin/dynamin-binding protein Abp1 link vesicle endocytosis to presynaptic active zones.* J Biol Chem, 2003. **278**(22): p. 20268-77.
142. Lipscombe, D., et al., *Spatial distribution of calcium channels and cytosolic calcium transients in growth cones and cell bodies of sympathetic neurons.* Proc Natl Acad Sci U S A, 1988. **85**(7): p. 2398-402.
143. Belardetti, F., et al., *The growth cones of Aplysia sensory neurons: Modulation by serotonin of action potential duration and single potassium channel currents.* Proc Natl Acad Sci U S A, 1986. **83**(18): p. 7094-8.
144. Belardetti, F., S. Schacher, and S.A. Siegelbaum, *Action potentials, macroscopic and single channel currents recorded from growth cones of Aplysia neurones in culture.* J Physiol, 1986. **374**: p. 289-313.
145. Gibson, G., L. Toral-Barza, and H. Zhang, *Selective changes in cell bodies and growth cones of nerve growth factor-differentiated PC12 cells induced by chemical hypoxia.* J Neurochem, 1997. **69**(2): p. 603-11.
146. Neely, M.D., *Role of substrate and calcium in neurite retraction of leech neurons following depolarization.* J Neurosci, 1993. **13**(3): p. 1292-301.
147. Neely, M.D. and M. Gesemann, *Disruption of microfilaments in growth cones following depolarization and calcium influx.* J Neurosci, 1994. **14**(12): p. 7511-20.
148. O'Lague, P.H., et al., *Morphological properties and membrane channels of the growth cones induced in PC12 cells by nerve growth factor.* J Neurosci Res, 1985. **13**(1-2): p. 301-21.
149. Wang, G.X. and M.M. Poo, *Requirement of TRPC channels in netrin-1-induced chemotropic turning of nerve growth cones.* Nature, 2005. **434**(7035): p. 898-904.
150. Wood, M.R., et al., *Plasmalemmal insertion and modification of sodium channels at the nerve growth cone.* J Neurosci, 1992. **12**(8): p. 2948-59.
151. Lockerbie, R.O., V.E. Miller, and K.H. Pfenninger, *Regulated plasmalemmal expansion in nerve growth cones.* J Cell Biol, 1991. **112**(6): p. 1215-27.
152. Hong, K. and M. Nishiyama, *From guidance signals to movement: signaling molecules governing growth cone turning.* Neuroscientist, 2010. **16**(1): p. 65-78.
153. Tojima, T., et al., *Second messengers and membrane trafficking direct and organize growth cone steering.* Nat Rev Neurosci, 2011. **12**(4): p. 191-203.
154. Henley, J. and M.-m. Poo, *Guiding neuronal growth cones using Ca2+ signals.* Trends in Cell Biology, 2004. **14**(6): p. 320-330.
155. Nelson, J.C., A.K. Stavoe, and D.A. Colón-Ramos, *The actin cytoskeleton in presynaptic assembly.* Cell Adh Migr, 2013. **7**(4): p. 379-87.
156. Omotade, O.F., S.L. Pollitt, and J.Q. Zheng, *Actin-based growth cone motility and guidance.* Mol Cell Neurosci, 2017. **84**: p. 4-10.
157. Schneider, F., I. Metz, and M.B. Rust, *Regulation of actin filament assembly and disassembly in growth cone motility and axon guidance.* Brain Res Bull, 2023. **192**: p. 21-35.
158. Wilson, E.S. and K. Newell-Litwa, *Stem cell models of human synapse development and degeneration.* Mol Biol Cell, 2018. **29**(24): p. 2913-2921.
159. Gong, X. and H. Wang, *SHANK1 and autism spectrum disorders.* Sci China Life Sci, 2015. **58**(10): p. 985-90.
160. Liu, Y.F., et al., *Autism and Intellectual Disability-Associated KIRREL3 Interacts with Neuronal Proteins MAP1B and MYO16 with Potential Roles in Neurodevelopment.* PLoS One, 2015. **10**(4): p. e0123106.
161. Guo, Y., et al., *Elevated levels of FMRP-target MAP1B impair human and mouse neuronal development and mouse social behaviors via autophagy pathway.* Nat Commun, 2023. **14**(1): p. 3801.

162. Walters, G.B., et al., *MAP1B mutations cause intellectual disability and extensive white matter deficit.* Nat Commun, 2018. **9**(1): p. 3456.
163. Moog, U. and K. Kutsche, *CASK Disorders*, in *GeneReviews(®)*, M.P. Adam, et al., Editors. 1993, University of Washington, SeattleCopyright © 1993-2023, University of Washington, Seattle. GeneReviews is a registered trademark of the University of Washington, Seattle. All rights reserved.: Seattle (WA).
164. Hackett, A., et al., *CASK mutations are frequent in males and cause X-linked nystagmus and variable XLMR phenotypes.* Eur J Hum Genet, 2010. **18**(5): p. 544-52.
165. Håvik, B., et al., *DCLK1 variants are associated across schizophrenia and attention deficit/hyperactivity disorder.* PLoS One, 2012. **7**(4): p. e35424.
166. Wu, J.Q., et al., *Transcriptome sequencing revealed significant alteration of cortical promoter usage and splicing in schizophrenia.* PLoS One, 2012. **7**(4): p. e36351.
167. Pinner, A.L., V. Haroutunian, and J.H. Meador-Woodruff, *Alterations of the myristoylated, alanine-rich C kinase substrate (MARCKS) in prefrontal cortex in schizophrenia.* Schizophr Res, 2014. **154**(1-3): p. 36-41.
168. Konopaske, G.T., et al., *Altered prefrontal cortical MARCKS and PPP1R9A mRNA expression in schizophrenia and bipolar disorder.* Schizophr Res, 2015. **164**(1-3): p. 100-8.
169. Zhao, Z., et al., *Association study of 167 candidate genes for schizophrenia selected by a multi-domain evidence-based prioritization algorithm and neurodevelopmental hypothesis.* PLoS One, 2013. **8**(7): p. e67776.
170. Fromer, M., et al., *De novo mutations in schizophrenia implicate synaptic networks.* Nature, 2014. **506**(7487): p. 179-84.
171. Lennertz, L., et al., *A promoter variant of SHANK1 affects auditory working memory in schizophrenia patients and in subjects clinically at risk for psychosis.* Eur Arch Psychiatry Clin Neurosci, 2012. **262**(2): p. 117-24.

Figures

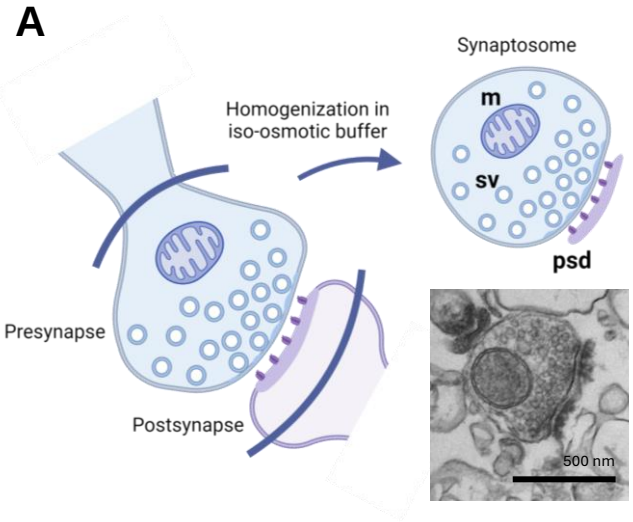

B

Synaptosomes enable the study of:

- **Neurotransmitter release and synaptic signaling** incl. PTM studies
- **Synapse omics** (e.g. lipidomics, proteomics)
- **Synaptic functionality** (Ca^{2+} dynamics, membrane potential etc.)
- **Synaptic plasticity**
- **Drug screening**
- **Disease modeling**
- **Comparative analysis** (brain regions, species, developmental stages etc.)
- **High-throughput screening** (biological, functional, drug assays)

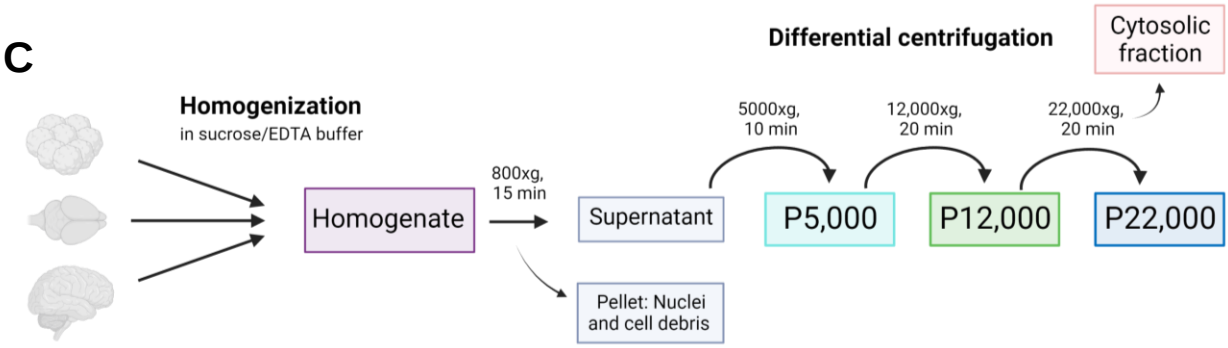

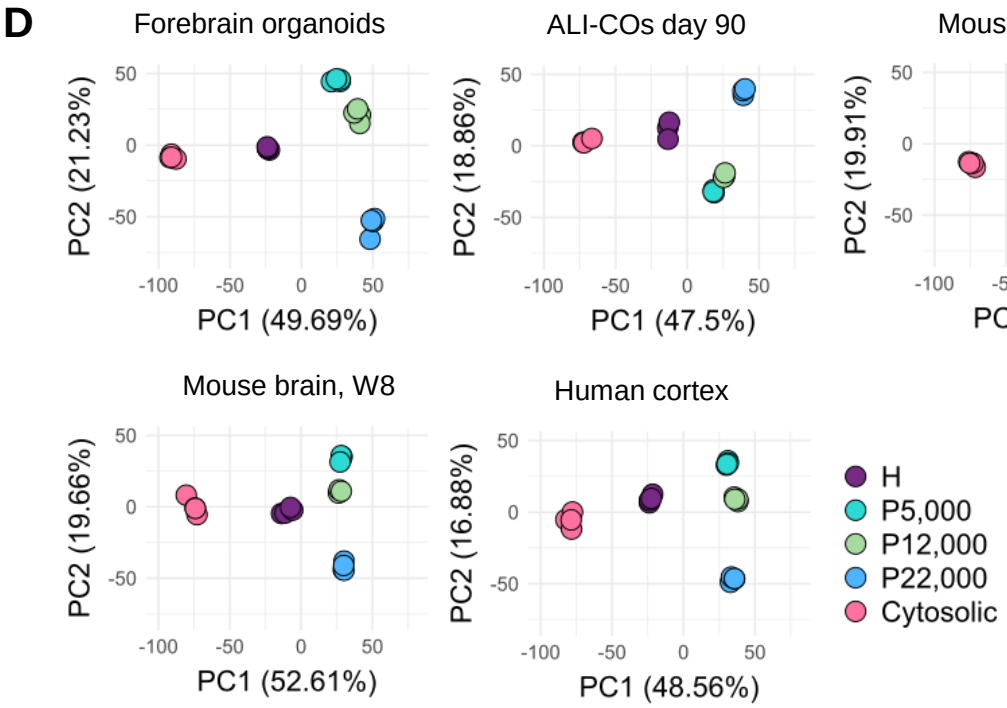

Figure 1: A) Schematic illustration of the formation of a synaptosome, including a TEM image of a mouse W8 synaptosome. m: mitochondrion, sv: synaptic vesicle, psd: postsynaptic density. **B)** List of examples of how synaptosomes can be used. PTM: Posttranslational modifications. **C)** Workflow of synaptosome enrichment using differential centrifugation. The differential centrifugation method was applied to forebrain organoids at day 100, ALI-COs at day 90, mouse brain at two developmental stages (postnatal day 2 (P2) and adult week 8 (W8)) and healthy cortical tissue from human brain. **D)** Proteomic data PCA plots showing technical replicates of the different fractions, homogenate (H), P5,000, P12,000, P22,000 and Cytosolic fraction, from differential centrifugation of human forebrain organoid tissue at day 99, ALI-COs at day 90, human cortical tissue and newborn (P2) or adult (W8) mouse brain tissue.

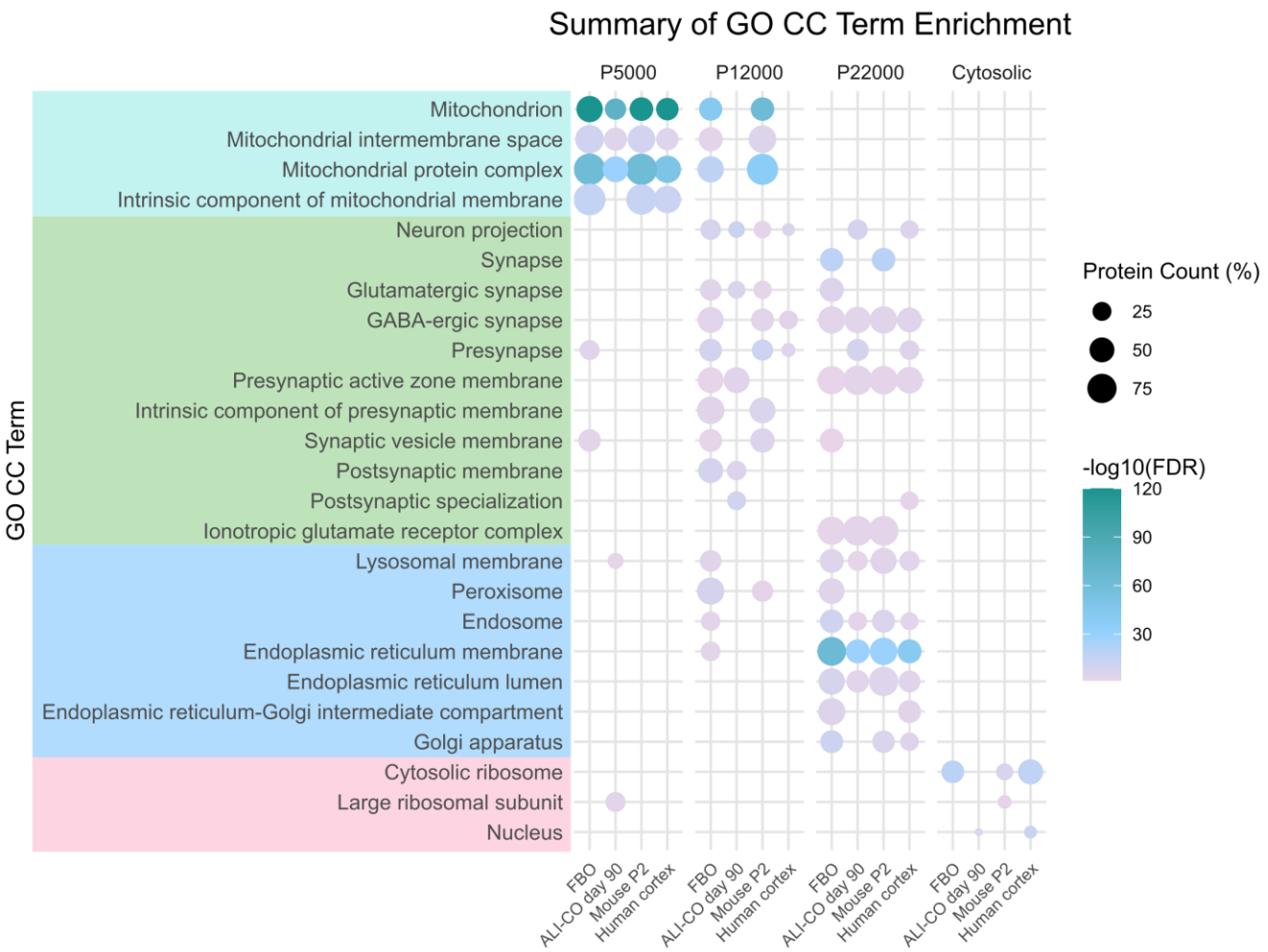

Figure 2: Summary of GO CC enrichment in the different fractions (Homogenate (H), P5,000, P12,000, P22,000 and Cytosolic) from the differential centrifugation protocol. The enrichment was based on fraction-specific proteins (FC ≥ 1.5 compared to homogenate, FDR ≤ 0.01) for each of the the four tissue types: forebrain organoids at day 100 (FBO), ALI-COs at day 90, mouse brain at postnatal day 2 (P2) and healthy cortical tissue from human brain (Human cortex). Mint: Mitochondrial terms; green: neuronal and synaptic terms; blue: endomembrane system terms; pink: cytosolic or nucleus terms. The terms were selected based on designated key-words (e.g. “synaptic”, “mitochondrial”, “lysosomal”, “golgi”, “cytosolic” etc.) together with the average FDR across tissue types, total number of proteins and number of times the term appeared across the datasets. All FDRs are below 0.05.

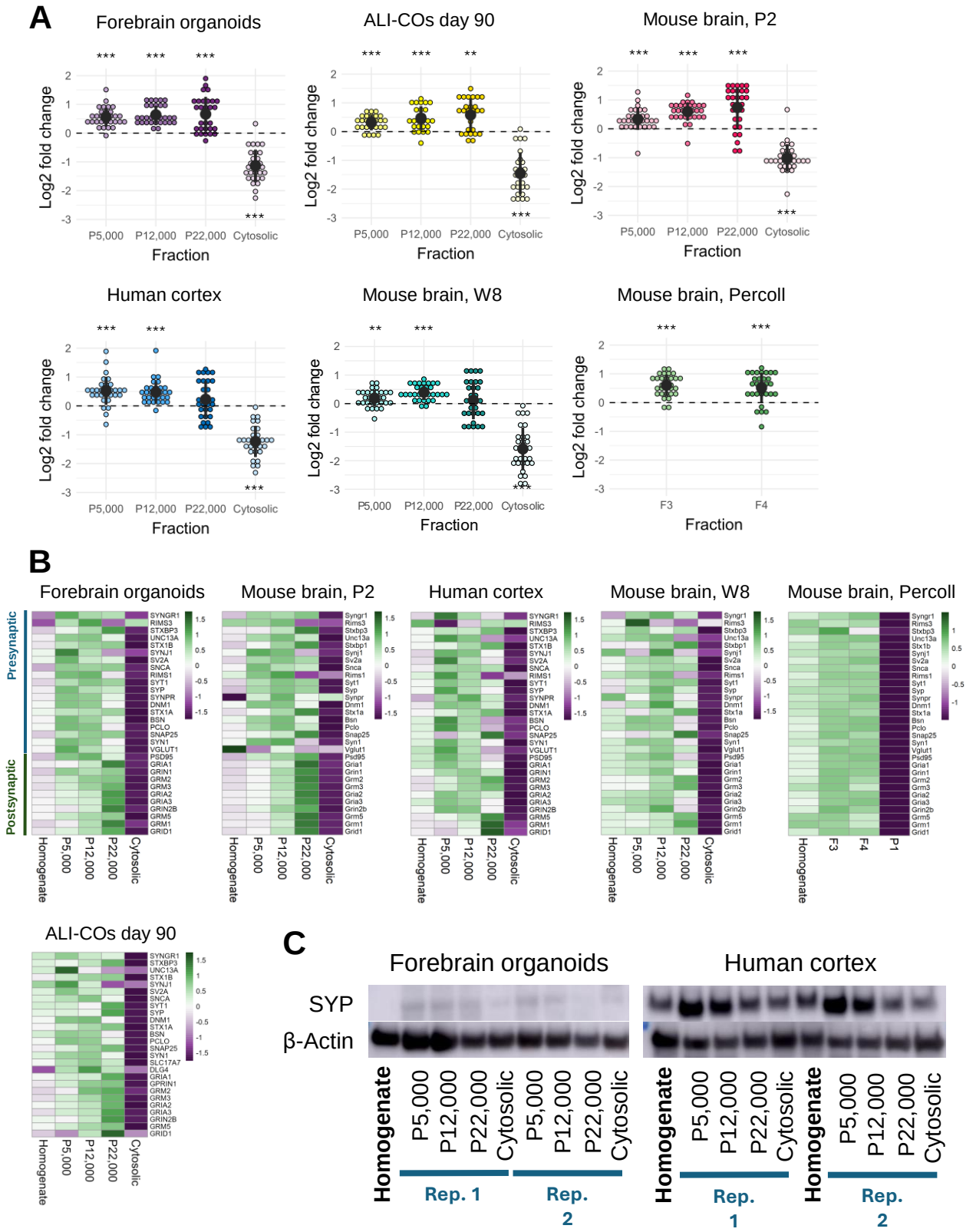

Figure 3: A) Changes in the levels of 30 selected synaptic markers in the differential centrifugation fractions compared to the homogenate from each tissue type. An enrichment of synaptosomes from adult mouse brain (W8) using the conventional Percoll® density gradient centrifugation method was performed in parallel to compare the synaptic protein enrichment levels. The conventional Percoll® F3 and F4 synaptosome enriched fractions are shown. **p < 0.001; ***p < 0.0001. **B)** Heatmaps of the normalized abundances of the same 30 synaptic markers as used in A for each fraction and tissue or enrichment type. P1: pellet from the first centrifugation, containing mainly whole cells, cell debris and nuclei to serve as a negative control. **C)** Western blots of the synaptic marker SYP in differential centrifugation fractions from human forebrain organoids and human cortical tissue.

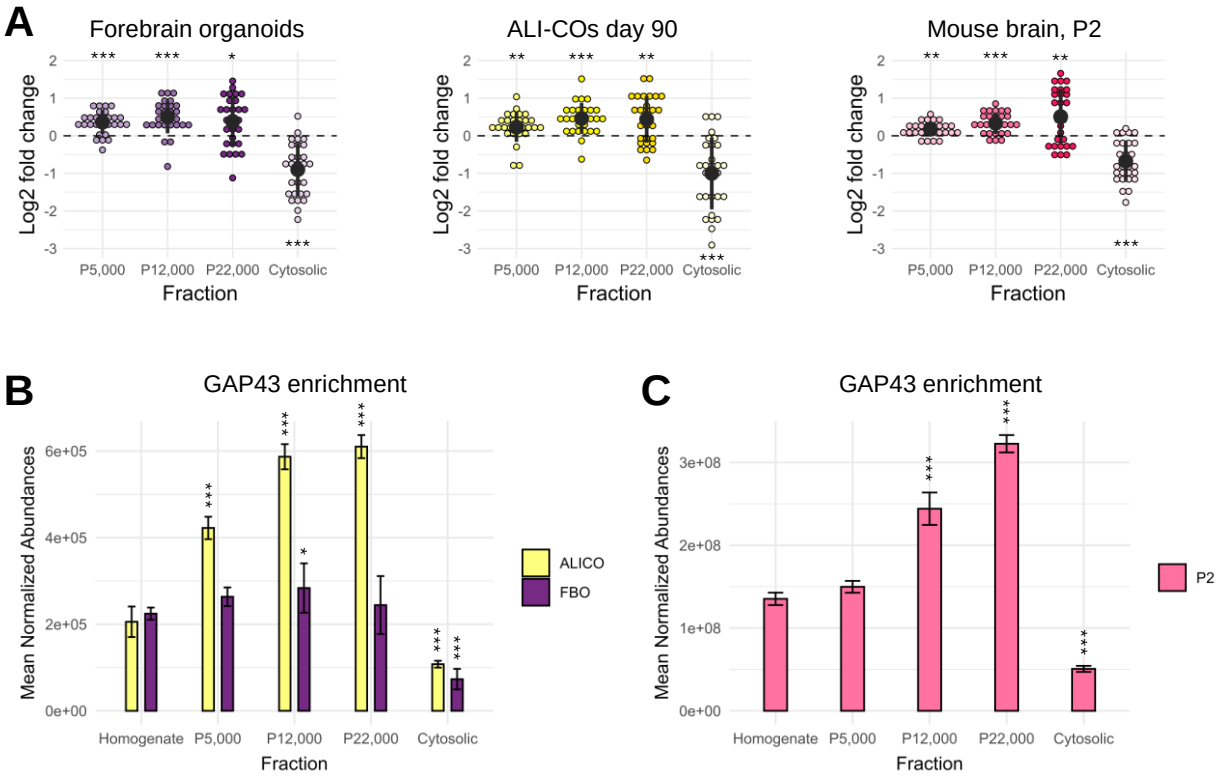

Figure 4) A) Levels of selected growth cone markers in the fractions compared to homogenate. The proteins were selected based on two other proteomic studies determining markers of growth cones. *p<0.01, **p < 0.001 and ***p < 0.0001. **B)** Abundance levels of the well-known growth cone marker GAP43 in the homogenate and the four fractions derived from ALICO day 90 and FBO and **C)** from newborn mouse brain (P2). Stars in **B** and **C** indicate significant FC compared to the corresponding Homogenate level with *p < 0.01 and ***p < 0.0001.

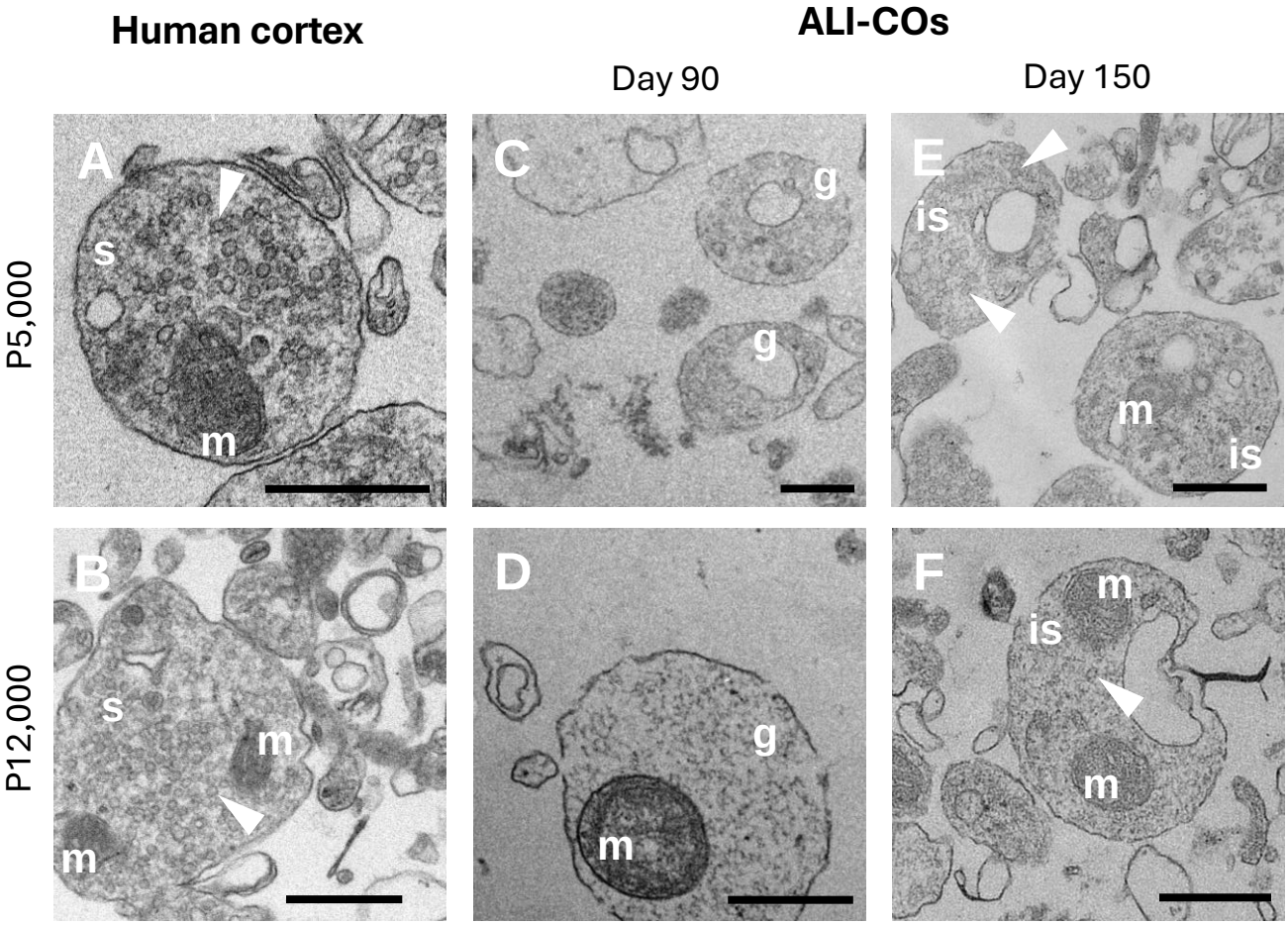

Figure 5: TEM images of differential centrifugation fractions from human cortex and ALI-COs at day 90 and 150. P5,000 and P12,000 fractions from human cortex **(A-B)** showing mature synaptosomes, and from ALI-COs **(C-F)** showing the presence of growth cone particles (GCPs) at day 90 and immature synaptosomes at day 150. Scalebars: 500nm. is: immature synaptosome, s: synaptosome, m: mitochondria, g: GCP, white arrows: synaptic vesicles.

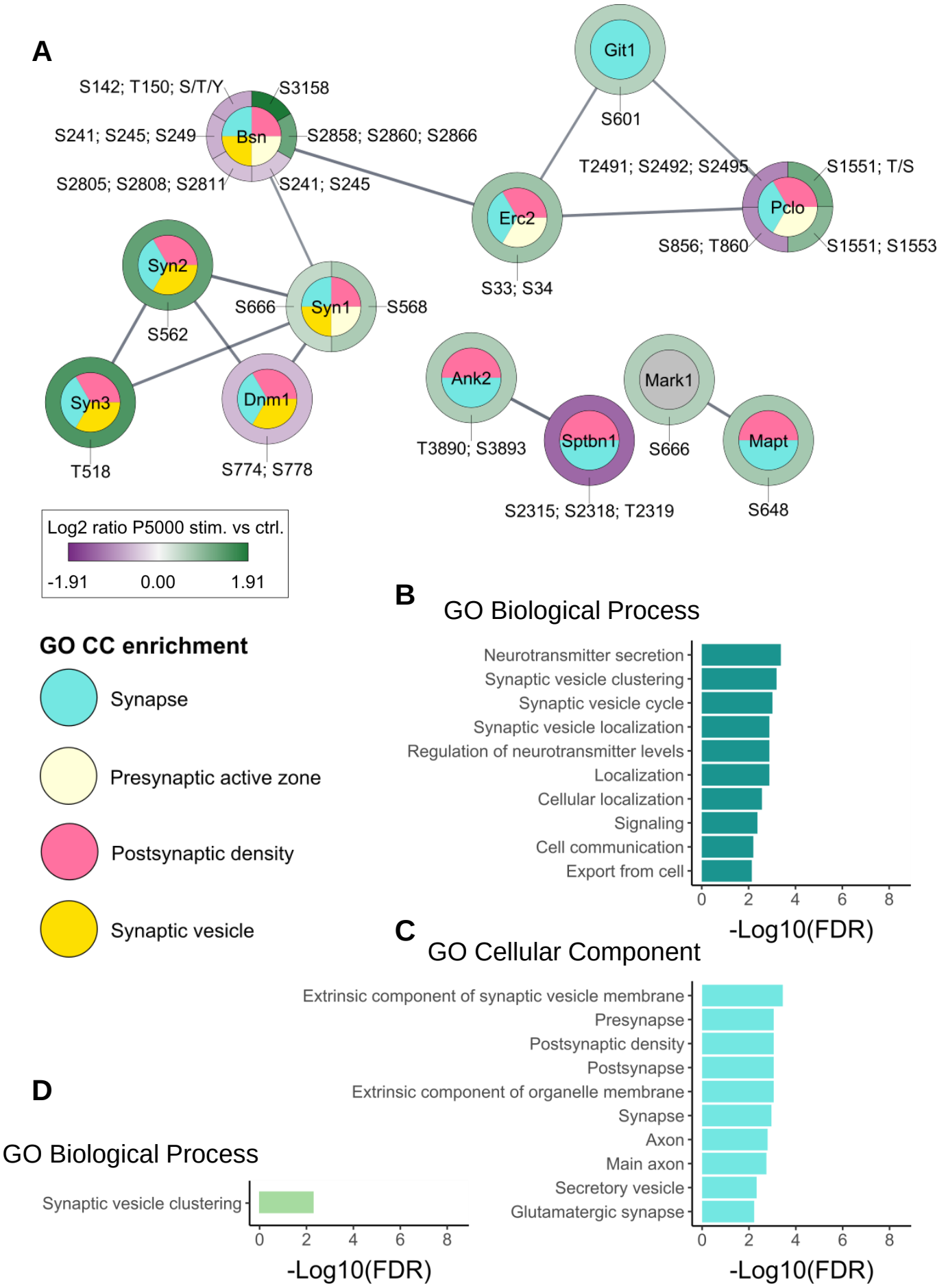
A
Git1
S601
S142; T150; S/T/Y
S3158
S241; S245; S249
Bsn
S2858; S2860; S2866
S2805; S2808; S2811
S241; S245
T2491; S2492; S2495
S1551; T/S
Erc2
Pclo
S856; T860
S1551; S1553
S33; S34
Syn2
S666
Syn1
S568
S562
Ank2
Mark1
Syn3
Dnm1
Sptbn1
Mapt
T3890; S3893
S666
T518
S774; S778
S2315; S2318; T2319
S648
Log2 ratio P5000 stim. vs ctrl.
-1.91
0.00
1.91
B
GO Biological Process
Neurotransmitter secretion
Synaptic vesicle clustering
Synaptic vesicle cycle
Synaptic vesicle localization
Regulation of neurotransmitter levels
Localization
Cellular localization
Signaling
Cell communication
Export from cell
0
2
4
6
8
-Log10(FDR)
GO CC enrichment
Synapse
Presynaptic active zone
Postsynaptic density
Synaptic vesicle
C
GO Cellular Component
Extrinsic component of synaptic vesicle membrane
Presynapse
Postsynaptic density
Postsynapse
Extrinsic component of organelle membrane
Synapse
Axon
Main axon
Secretory vesicle
Glutamatergic synapse
0
2
4
6
8
-Log10(FDR)
D
GO Biological Process
Synaptic vesicle clustering
0
2
4
6
8
-Log10(FDR)

Figure 6: A) High KCl stimulation-related changes in protein phosphorylation (FC ≥ 1.3 up or down, FDR ≤ 0.05) of adult mouse synaptosomes from the P5,000 fraction generated with the differential centrifugation method described. Proteins belonging to the GO Cellular Component enriched terms "Synapse", "Postsynaptic density", "Presynaptic active zone", and "Synaptic vesicle" are marked in different colors. STRING networks showing connected nodes only (confidence score cutoff: 0.7). **B-C)** GO Biological Process and Cellular Component term enrichment for proteins with stimulation-related changes in phosphorylation for the differential centrifugation derived P5,000 **(B-C)** and P12,000 **(D)** fractions. Top 10 terms showed, FDR ≤ 0.05.

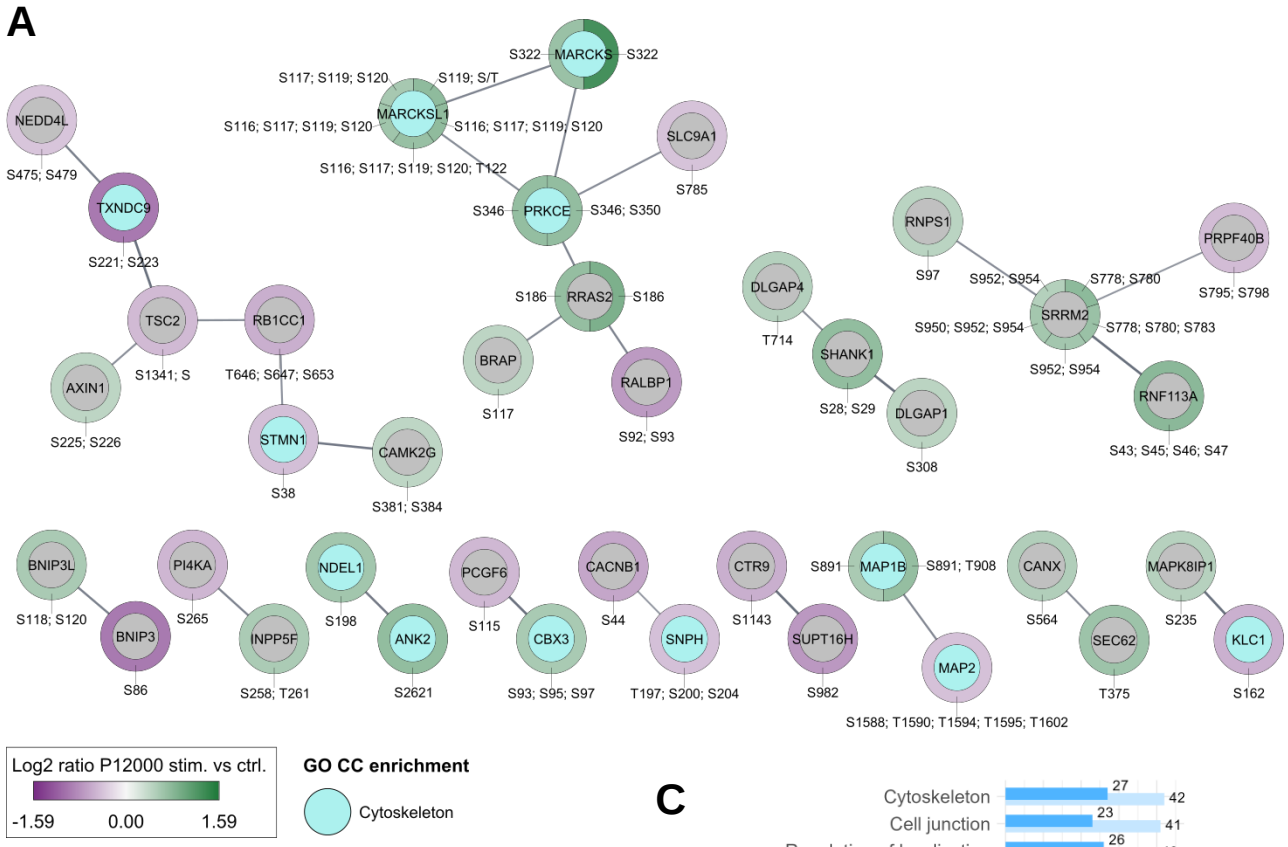
A
MARCKS
S322
S322
MARCKSL1
S117; S119; S120
S119; S/T
S116; S117; S119; S120
S116; S117; S119; S120
S116; S117; S119; S120; T122
NEDD4L
S475; S479
TXNDC9
S221; S223
SLC9A1
S785
PRKCE
S346
S346; S350
RRAS2
S186
S186
BRAP
S117
RALBP1
S92; S93
TSC2
S1341; S
RB1CC1
T646; S647; S653
AXIN1
S225; S226
STMN1
S38
CAMK2G
S381; S384
RNPS1
S97
PRPF40B
S795; S798
S952; S954
S778; S780
SRRM2
S950; S952; S954
S778; S780; S783
S952; S954
RNF113A
S43; S45; S46; S47
DLGAP4
T714
SHANK1
S28; S29
DLGAP1
S308
BNIP3L
S118; S120
BNIP3
S86
PI4KA
S265
INPP5F
S258; T261
NDEL1
S198
ANK2
S2621
PCGF6
S115
CBX3
S93; S95; S97
CACNB1
S44
SNPH
T197; S200; S204
CTR9
S1143
SUPT16H
S982
S891
MAP1B
S891; T908
MAP2
S1588; T1590; T1594; T1595; T1602
CANX
S564
SEC62
T375
MAPK8IP1
S235
KLC1
S162
Log2 ratio P12000 stim. vs ctrl.
-1.59
0.00
1.59
GO CC enrichment
Cytoskeleton

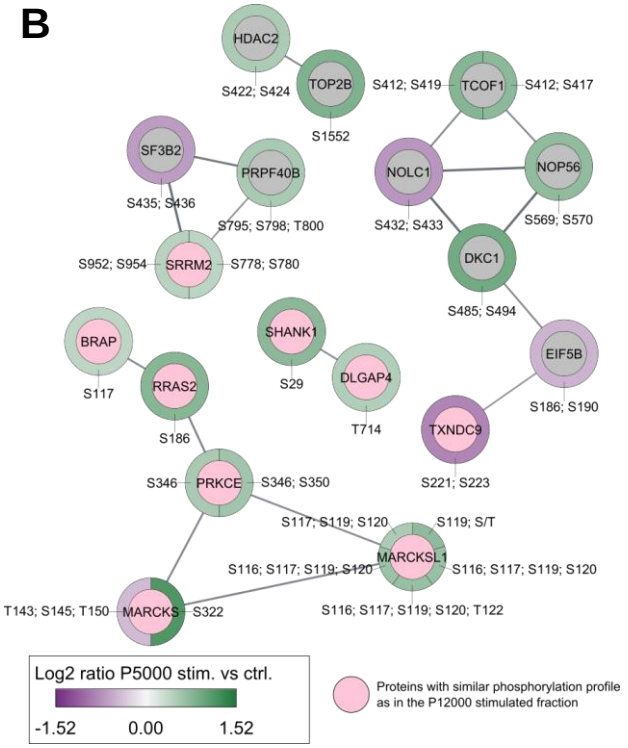
B
HDAC2
S422; S424
TOP2B
S1552
S412; S419
TCOF1
S412; S417
SF3B2
S435; S436
PRPF40B
S795; S798; T800
NOLC1
S432; S433
NOP56
S569; S570
S952; S954
SRRM2
S778; S780
DKC1
S485; S494
BRAP
S117
RRAS2
S186
SHANK1
S29
DLGAP4
T714
EIF5B
S186; S190
TXNDC9
S221; S223
S346
PRKCE
S346; S350
S117; S119; S120
S119; S/T
MARCKSL1
S116; S117; S119; S120
S116; S117; S119; S120
S116; S117; S119; S120; T122
T143; S145; T150
MARCKS
S322
Log2 ratio P5000 stim. vs ctrl.
-1.52
0.00
1.52
Proteins with similar phosphorylation profile as in the P12000 stimulated fraction

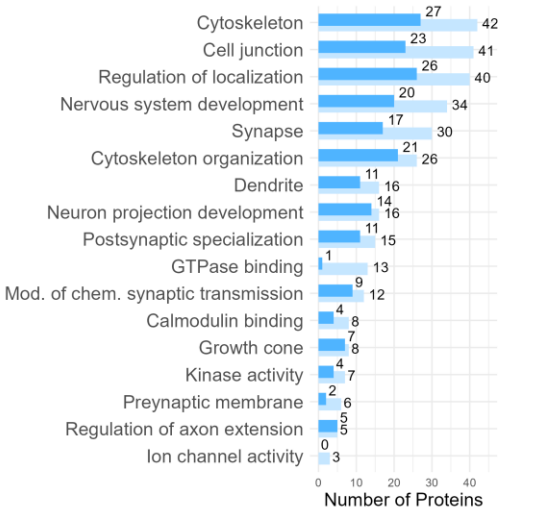
C
Cytoskeleton
Cell junction
Regulation of localization
Nervous system development
Synapse
Cytoskeleton organization
Dendrite
Neuron projection development
Postsynaptic specialization
GTPase binding
Mod. of chem. synaptic transmission
Calmodulin binding
Growth cone
Kinase activity
Preynaptic membrane
Regulation of axon extension
Ion channel activity
27
42
23
41
26
40
20
34
17
30
21
26
11
16
14
16
11
15
1
13
9
12
4
8
7
8
4
7
2
6
5
5
0
3
0
10
20
30
40
Number of Proteins
Fraction
P12,000
P5,000

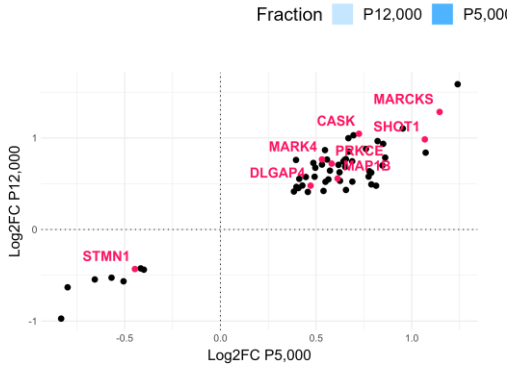
D
MARCKS
CASK
SHOT1
MARK4
PRKCE
DLGAP4
MAP1B
STMN1
Log2FC P12,000
Log2FC P5,000
1
0
-1
-0.5
0.0
0.5
1.0

Figure 7: A-B) High KCl stimulation-related changes in protein phosphorylation (FC ≥ 1.3 up or down, FDR ≤ 0.05) in the **A)** P12,000 or **B)** P5,000 fractions from 90 days old ALI-COs subjected to the differential centrifugation method. Proteins belonging to the GO Cellular Component enriched term "Cytoskeleton" (FDR: 0.0046) are marked in blue in **A)**. Proteins with similar phosphorylation profile between the two fractions are marked in pink in **B)**. PPI STRING networks showing connected nodes only (confidence score cutoff: 0.7). **C)** GO terms and annotated number of proteins with regulation in phosphorylation for each fraction P5,000 and P12,000. The terms were not significantly enriched (except "Cytoskeleton" for P12,000), but provides an overview of which kinds of pathways the protein phosphorylation changes appear in. The total number of proteins with regulation in phosphorylation was: P12,000: 133 and P5,000: 82. **D)** Correlation plot of Log2 fold changes for the significantly regulated phosphopeptides present in both the P5,000 and P12,000 fractions (n=59). Pearson's correlation coefficient: 0.94, P-value: 3.58E-29. Protein names of a few selected peptides are marked in pink.

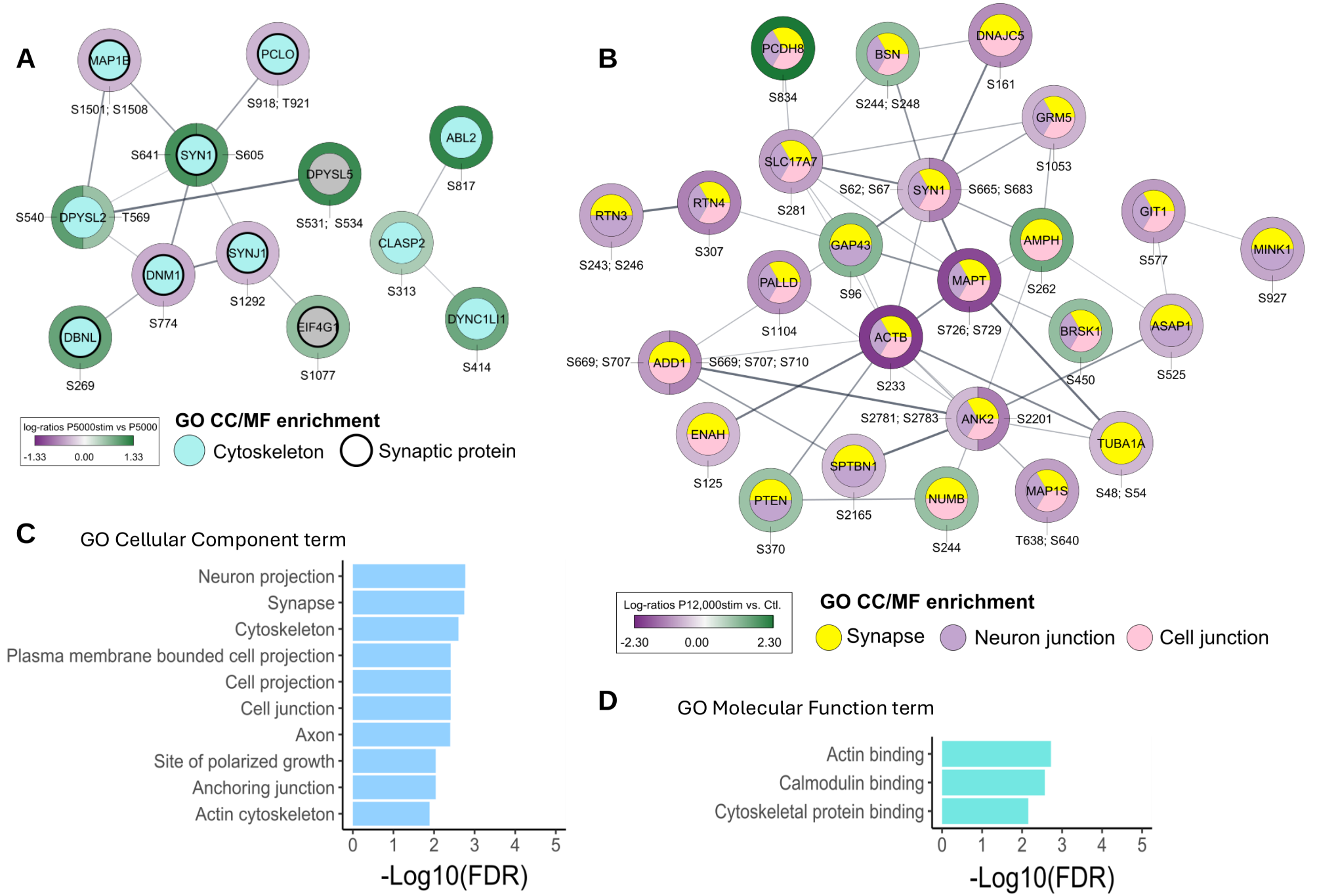
A
MAP1B
S1501; S1508
PCLO
S918; T921
S641
SYN1
S605
DPYSL5
S531; S534
ABL2
S817
S540
DPYSL2
T569
CLASP2
S313
SYNJ1
S1292
DNM1
S774
DBNL
S269
EIF4G1
S1077
DYNC1LI1
S414
log-ratios P5000stim vs P5000
-1.33
0.00
1.33
GO CC/MF enrichment
Cytoskeleton
Synaptic protein
B
PCDH8
S834
BSN
S244; S248
DNAJC5
S161
GRM5
S1053
SLC17A7
S281
S62; S67
SYN1
S665; S683
RTN3
S243; S246
RTN4
S307
GAP43
S96
AMPH
S262
GIT1
S577
MINK1
S927
PALLD
S1104
MAPT
S726; S729
ACTB
S233
BRSK1
S450
ASAP1
S525
S669; S707
ADD1
S669; S707; S710
S2781; S2783
ANK2
S2201
ENAH
S125
TUBA1A
S48; S54
SPTBN1
S2165
PTEN
S370
NUMB
S244
MAP1S
T638; S640
Log-ratios P12,000stim vs. Ctl.
-2.30
0.00
2.30
GO CC/MF enrichment
Synapse
Neuron junction
Cell junction
C
GO Cellular Component term
Neuron projection
Synapse
Cytoskeleton
Plasma membrane bounded cell projection
Cell projection
Cell junction
Axon
Site of polarized growth
Anchoring junction
Actin cytoskeleton
0
1
2
3
4
5
-Log10(FDR)
D
GO Molecular Function term
Actin binding
Calmodulin binding
Cytoskeletal protein binding
0
1
2
3
4
5
-Log10(FDR)

Figure 8: A) High KCl stimulation-related changes in protein phosphorylation (FC ≥ 1.3 up or down, FDR ≤ 0.20) in the 5,000 fraction from 150 days old ALI-COs subjected to the differential centrifugation method. Proteins belonging to the GO Cellular Component enriched term "Cytoskeleton" (FDR: 0.0089) are marked in blue and synaptic proteins are marked with a black circle. **B)** High KCl stimulation related changes in protein phosphorylation (FC ≥ 1.3 up or down, FDR ≤ 0.20) of proteins belonging to the GO CC term "Synapse" in the 12,000 fraction from 150 days old ALI-COs. **A-B** PPI STRING networks showing connected nodes only (confidence score cutoff: 0.4). **C-D)** Top-10 GO Cellular Component and Molecular Function terms enriched among the P12,000 proteins with changes in phosphorylation (FC ≥ 1.3 up or down, FDR ≤ 0.20).

Supplementary

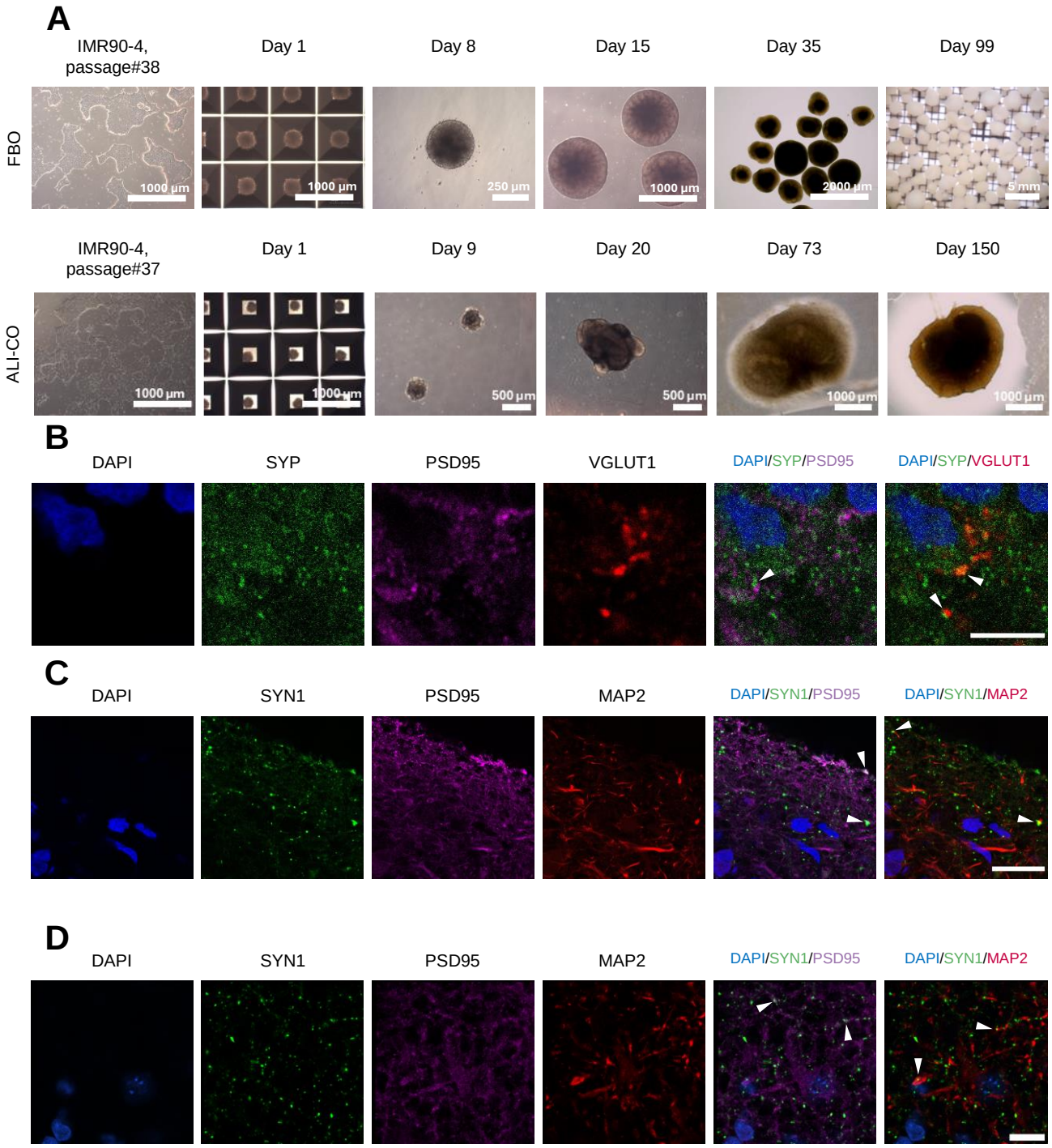

Figure S1: A) Light microscopic images of IMR90-4 IPSCs and forebrain organoids or ALI-COs at different differentiation stages. **B-C)** Immunohistochemical (IHC) labelling of synapses in forebrain organoids at day 100. **B)** Labelling of presynaptic markers Synaptophysin (SYP) and Vesicular glutamate transporter 1 (VGLUT1) and postsynaptic marker Postsynaptic density protein 95 (PSD95) at day 99. Scalebar: 5µm. **C)** Labelling of presynaptic marker Synapsin 1 (SYN1), postsynaptic marker PSD95 and dendritic marker Microtubule associated protein 2 (MAP2) at day 100. Scalebar: 20µm. **D)** ALI-COs labeled at day 100 for same markers as in **C**. Scale bar: 10µm. White arrows pointing at areas with co-localization or adjacent expression of the pre- and postsynaptic markers. For all IHC images, n=3.

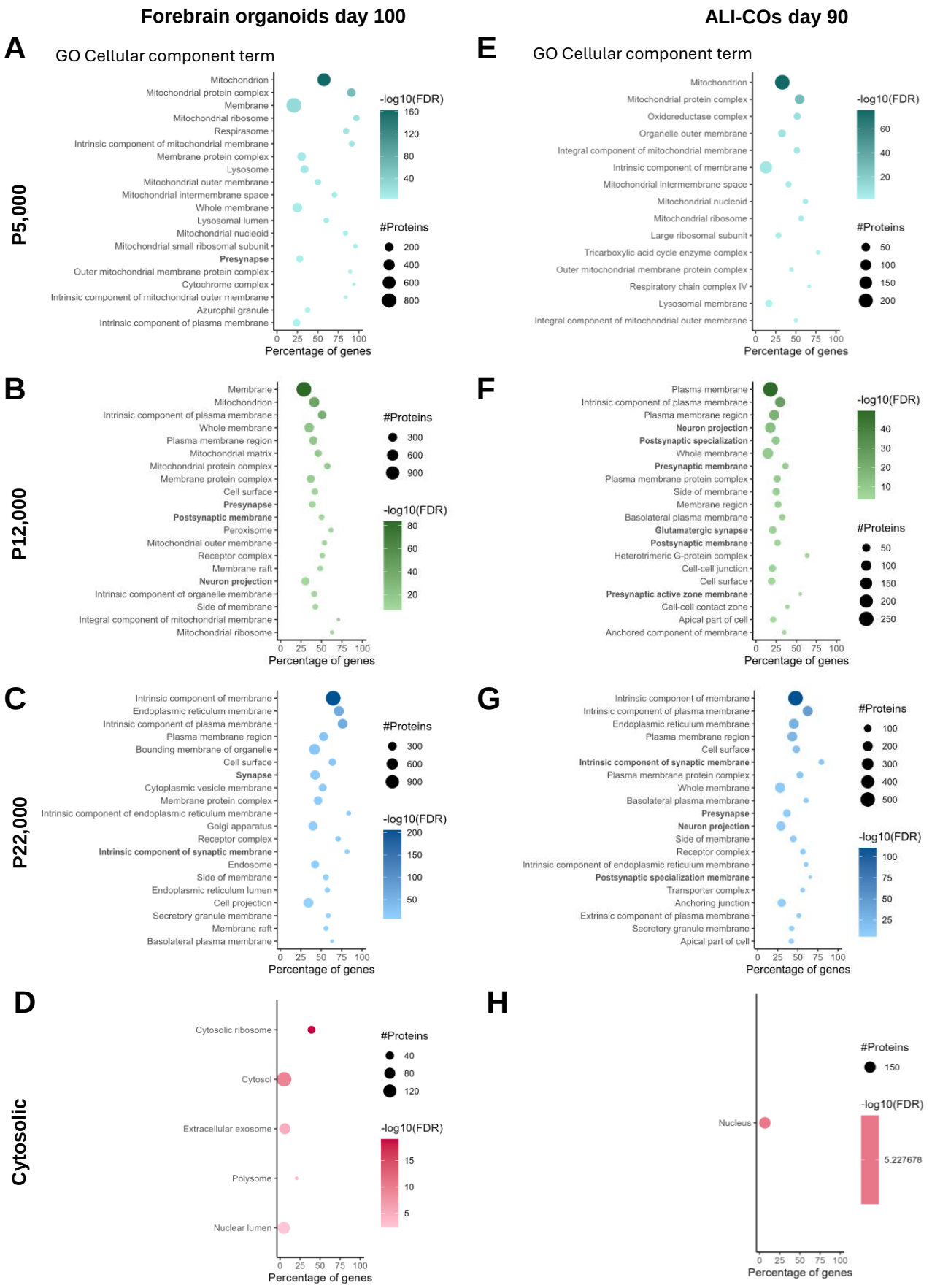
Forebrain organoids day 100
ALI-COs day 90
A
GO Cellular component term
P5,000
Mitochondrion
Mitochondrial protein complex
Membrane
Mitochondrial ribosome
Respirasome
Intrinsic component of mitochondrial membrane
Membrane protein complex
Lysosome
Mitochondrial outer membrane
Mitochondrial intermembrane space
Whole membrane
Lysosomal lumen
Mitochondrial nucleoid
Mitochondrial small ribosomal subunit
Presynapse
Outer mitochondrial membrane protein complex
Cytochrome complex
Intrinsic component of mitochondrial outer membrane
Azurophil granule
Intrinsic component of plasma membrane
-log10(FDR)
160
120
80
40
#Proteins
200
400
600
800
0 25 50 75 100
Percentage of genes
E
GO Cellular component term
Mitochondrion
Mitochondrial protein complex
Oxidoreductase complex
Organelle outer membrane
Integral component of mitochondrial membrane
Intrinsic component of membrane
Mitochondrial intermembrane space
Mitochondrial nucleoid
Mitochondrial ribosome
Large ribosomal subunit
Tricarboxylic acid cycle enzyme complex
Outer mitochondrial membrane protein complex
Respiratory chain complex IV
Lysosomal membrane
Integral component of mitochondrial outer membrane
-log10(FDR)
60
40
20
#Proteins
50
100
150
200
0 25 50 75 100
Percentage of genes
B
P12,000
Membrane
Mitochondrion
Intrinsic component of plasma membrane
Whole membrane
Plasma membrane region
Mitochondrial matrix
Mitochondrial protein complex
Membrane protein complex
Cell surface
Presynapse
Postsynaptic membrane
Peroxisome
Mitochondrial outer membrane
Receptor complex
Membrane raft
Neuron projection
Intrinsic component of organelle membrane
Side of membrane
Integral component of mitochondrial membrane
Mitochondrial ribosome
#Proteins
300
600
900
-log10(FDR)
80
60
40
20
0 25 50 75 100
Percentage of genes
F
Plasma membrane
Intrinsic component of plasma membrane
Plasma membrane region
Neuron projection
Postsynaptic specialization
Whole membrane
Presynaptic membrane
Plasma membrane protein complex
Side of membrane
Membrane region
Basolateral plasma membrane
Glutamatergic synapse
Postsynaptic membrane
Heterotrimeric G-protein complex
Cell-cell junction
Cell surface
Presynaptic active zone membrane
Cell-cell contact zone
Apical part of cell
Anchored component of membrane
-log10(FDR)
40
30
20
10
#Proteins
50
100
150
200
250
0 25 50 75 100
Percentage of genes
C
P22,000
Intrinsic component of membrane
Endoplasmic reticulum membrane
Intrinsic component of plasma membrane
Plasma membrane region
Bounding membrane of organelle
Cell surface
Synapse
Cytoplasmic vesicle membrane
Membrane protein complex
Intrinsic component of endoplasmic reticulum membrane
Golgi apparatus
Receptor complex
Intrinsic component of synaptic membrane
Endosome
Side of membrane
Endoplasmic reticulum lumen
Cell projection
Secretory granule membrane
Membrane raft
Basolateral plasma membrane
#Proteins
300
600
900
-log10(FDR)
200
150
100
50
0 25 50 75 100
Percentage of genes
G
Intrinsic component of membrane
Intrinsic component of plasma membrane
Endoplasmic reticulum membrane
Plasma membrane region
Cell surface
Intrinsic component of synaptic membrane
Plasma membrane protein complex
Whole membrane
Basolateral plasma membrane
Presynapse
Neuron projection
Side of membrane
Receptor complex
Intrinsic component of endoplasmic reticulum membrane
Postsynaptic specialization membrane
Transporter complex
Anchoring junction
Extrinsic component of plasma membrane
Secretory granule membrane
Apical part of cell
#Proteins
100
200
300
400
500
-log10(FDR)
100
75
50
25
0 25 50 75 100
Percentage of genes
D
Cytosolic
Cytosolic ribosome
Cytosol
Extracellular exosome
Polysome
Nuclear lumen
#Proteins
40
80
120
-log10(FDR)
15
10
5
0 25 50 75 100
Percentage of genes
H
Nucleus
#Proteins
150
-log10(FDR)
5.227678
0 25 50 75 100
Percentage of genes

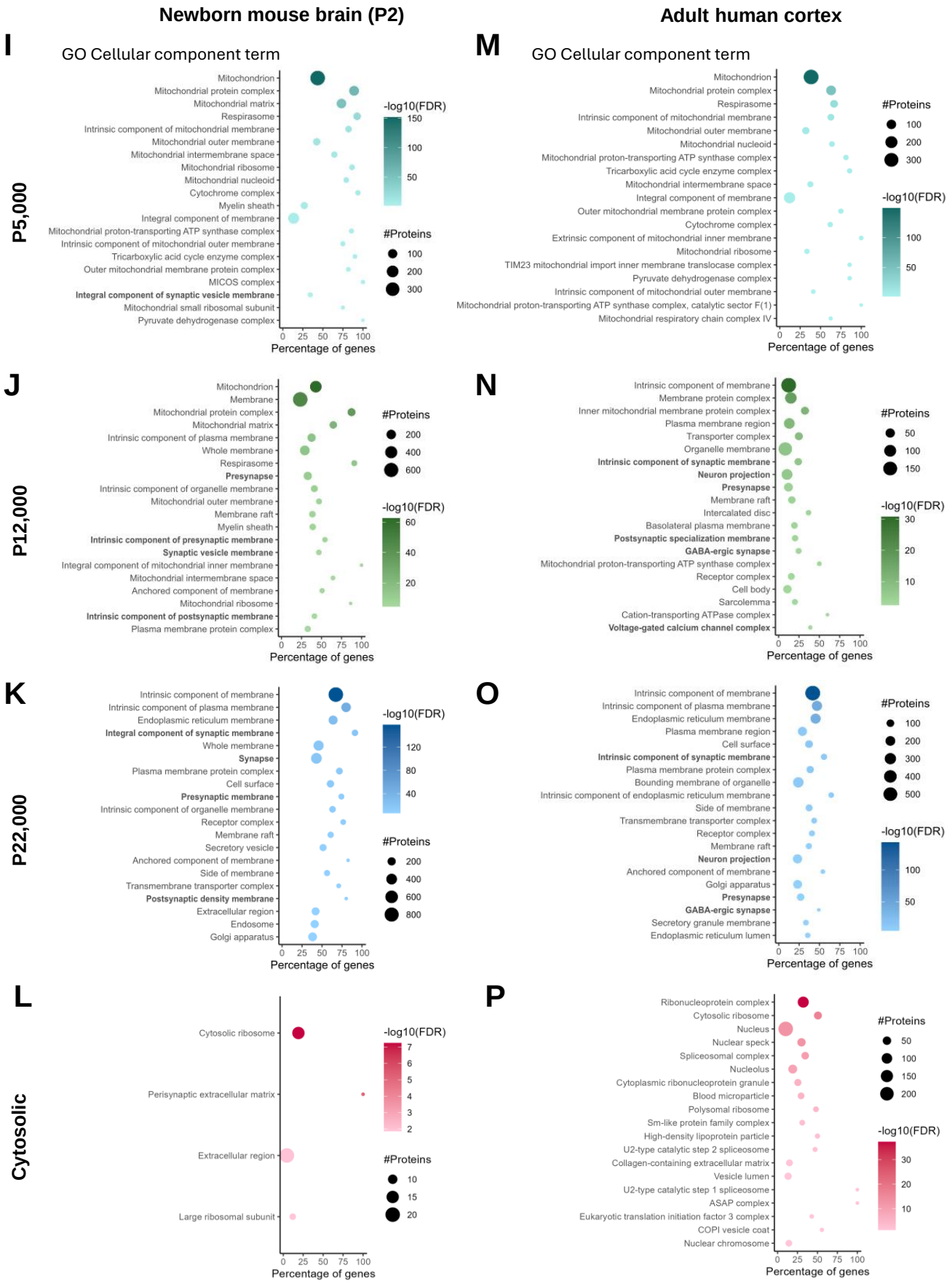

Figure S2: A-P GO Cellular Component enriched terms (top 20, FDR ≤ 0.05) based on fraction-specific proteins (FC ≥ 1.5 compared to homogenate, FDR ≤ 0.01). P5,000, P12,000, P22,000 and Cytosolic fractions from differential centrifugation of Forebrain organoids (day 100), ALI-COs (day 90), newborn mouse brain tissue (postnatal day 2 (P2)) and surgery derived adult human cortical tissue.

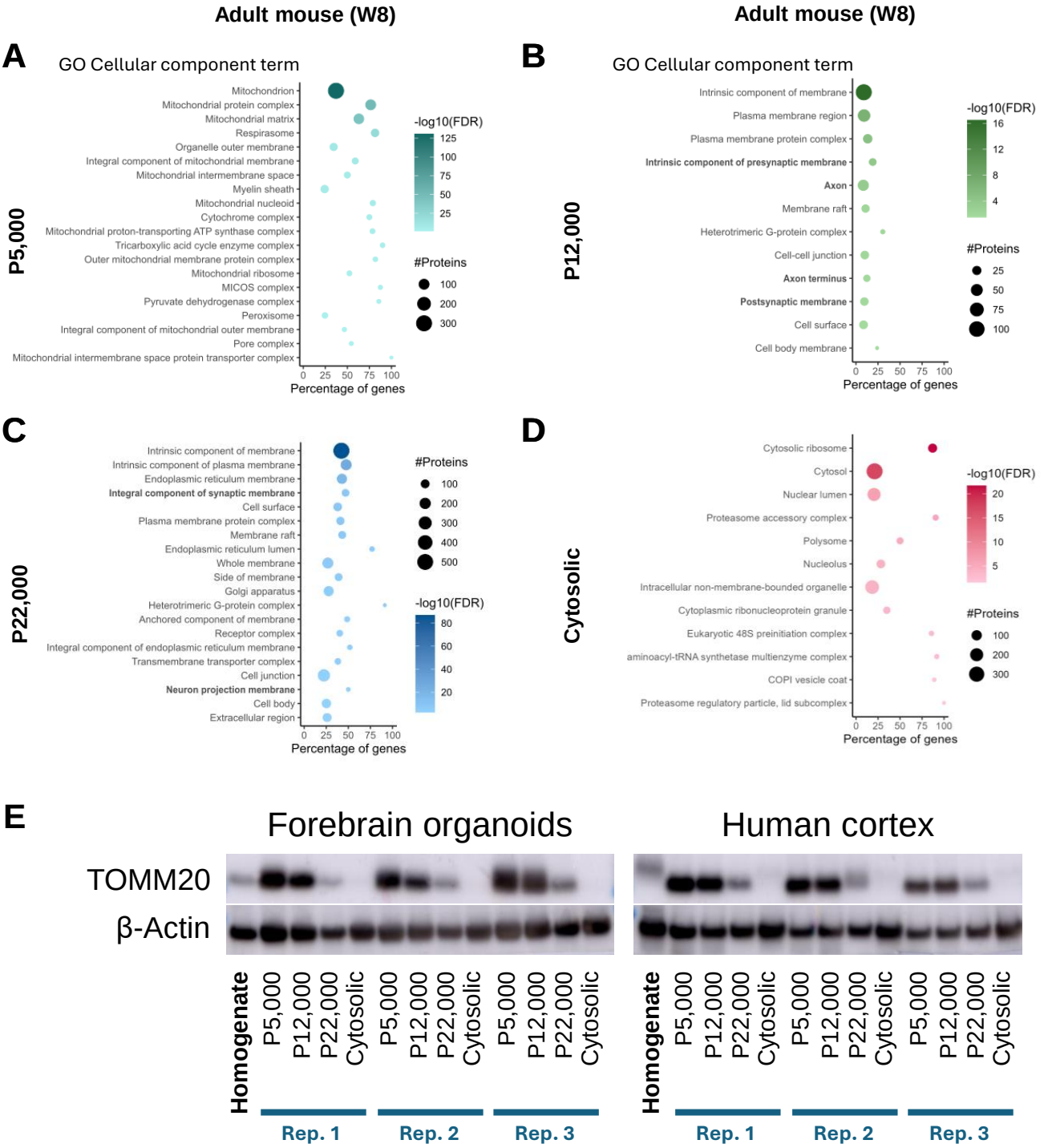

Figure S3: A-D GO Cellular Component enriched terms (top 20, FDR ≤ 0.05) based on fraction specific proteins (FC ≥ 1.5 compared to homogenate, FDR ≤ 0.01). P5,000, P12,000, P22,000 and Cytosolic fractions from differential centrifugation of adult mouse brain tissue (W8). **E)** Western blot of the mitochondrial marker TOMM20 in differential centrifugation fractions from forebrain organoids and human cortex in three technical replicates of the centrifugation.

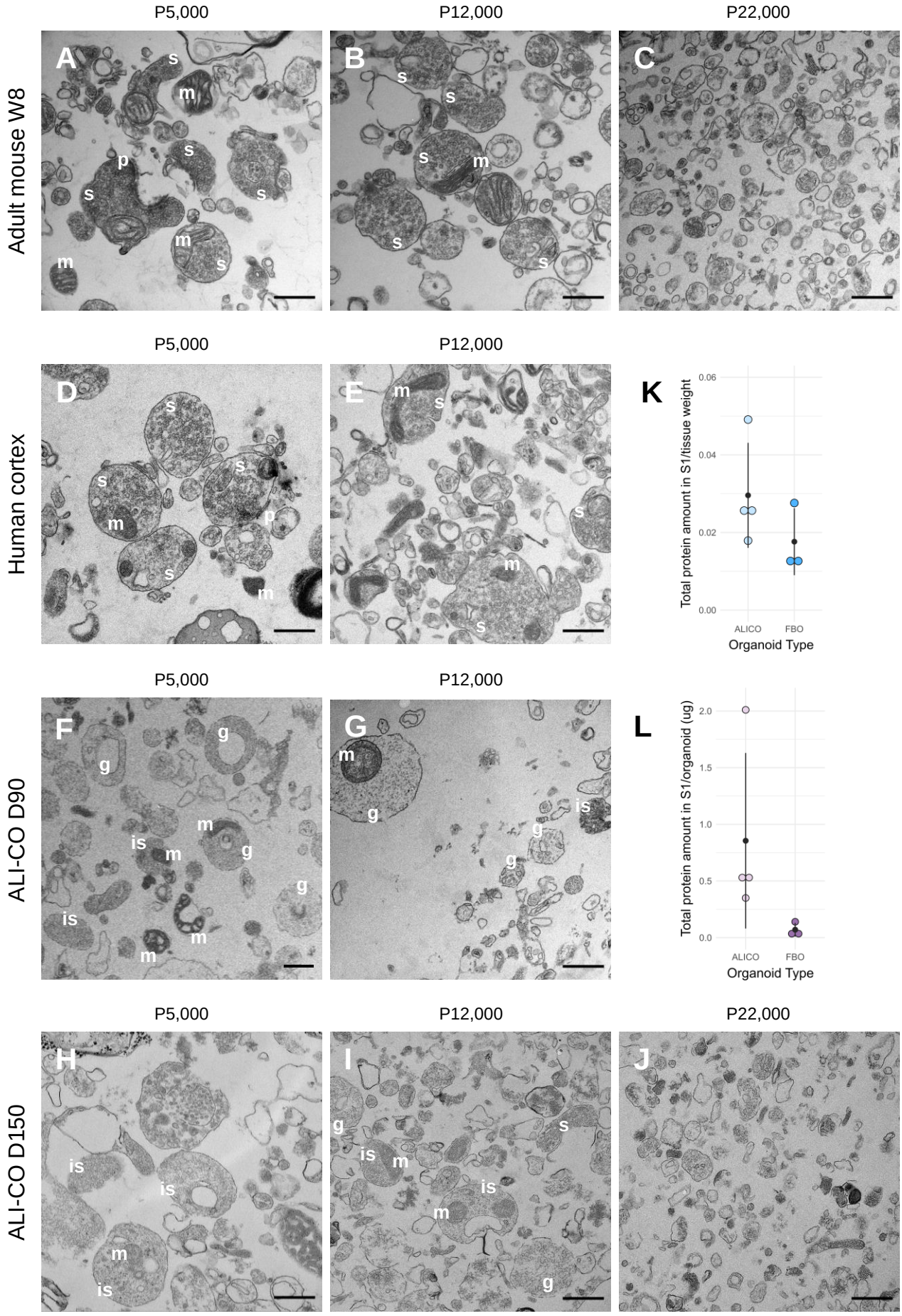
P5,000
P12,000
P22,000
Adult mouse W8
A
B
C
P5,000
P12,000
Human cortex
D
E
K
Total protein amount in S1/tissue weight
0.06
0.04
0.02
0.00
ALICO
FBO
Organoid Type
P5,000
P12,000
ALI-CO D90
F
G
L
Total protein amount in S1/organoid (ug)
2.0
1.5
1.0
0.5
0.0
ALICO
FBO
Organoid Type
P5,000
P12,000
P22,000
ALI-CO D150
H
I
J

Figure S4: A-J) TEM images of differential centrifugation fractions from adult mouse, adult human cortex and ALI-COs day 90 and 150. **A-C)** Adult mouse fractions P5,000, P12,000 and P22,000. Synaptosomes (s) are clearly present in the P5,000 and P12,000 fractions. The P22,000 fraction contains mainly smaller undefined membrane structures. **D-E)** Human cortex fractions P5,000, P12,000. Synaptosomes are clearly visible in both fractions. **F-G)** Day 90 ALI-CO fractions P5,000, P12,000. A few synaptosomes or immature synaptosomes (is) could be seen, however, many structures resembled growth cone particles (g). **H-J)** Day 150 ALI-CO fractions P5,000, P12,000 and P22,000. Immature synaptosomes are seen in the P5,000 and P12,000 fractions with the presence of mitochondria and some synaptic vesicles. Scalebars **A-J)**: 500nm. s: synaptosome, is: immature synaptosome, m: mitochondria, g: growth cone particle (GCP). **K-L)** Comparison of yield from the differential centrifugation between ALI-CO (slice-culture) and FBO (spherical culture) organoids. **K)** Total protein amount (µg) in the first supernatant (S1) used for differential centrifugation per total weight of the used organoid tissue and **L)** per number of organoids used to begin with. The number of ALI-COs is corrected assuming that each initial cerebral organoid generates at least 4 ALICO slices.

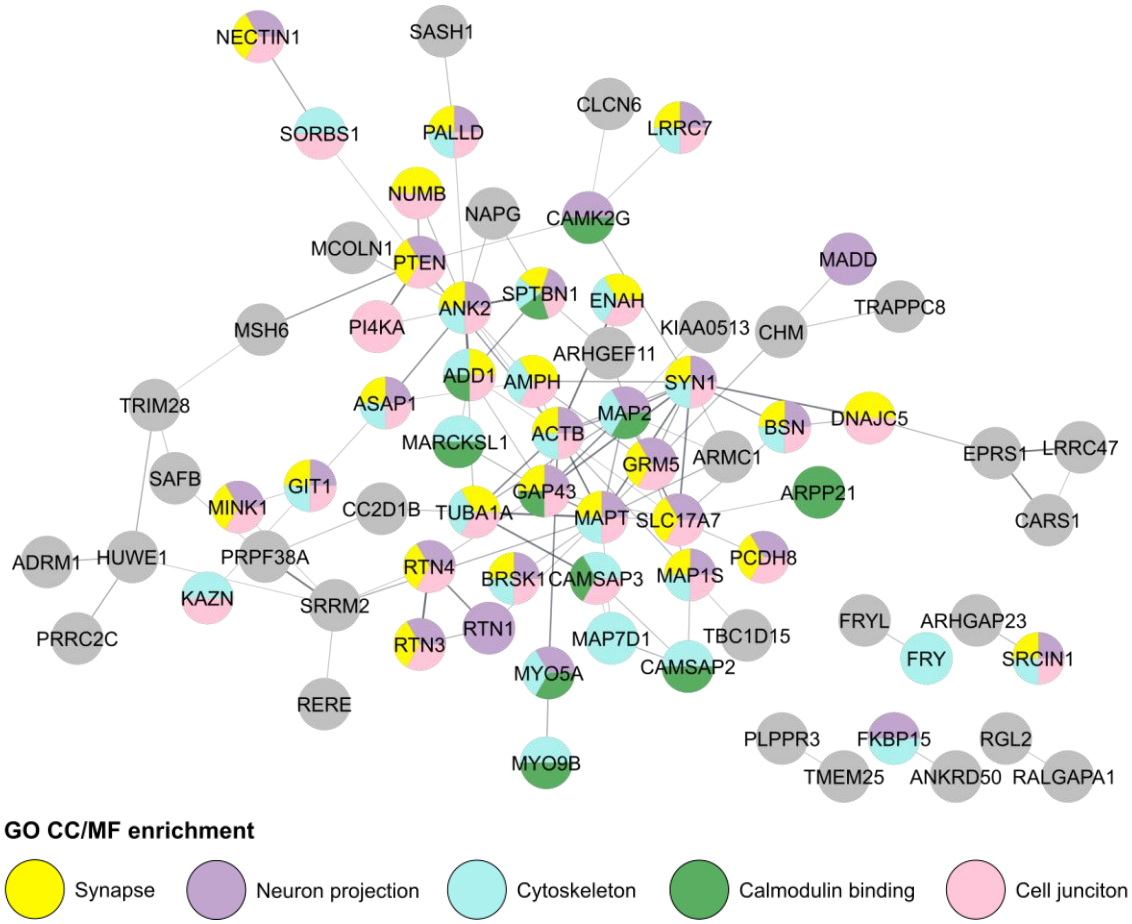

Figure S5: PPI of proteins with changes in phosphorylation (FC ≥ 1.3 up or down, Limma FDR ≤ 0.20) in the P12,000 fraction from 150 days old ALI-COs subjected to the differential centrifugation method. Proteins belonging to the GO CC or MF enriched terms "Synapse", "Neuron Projection", "Cytoskeleton", "Calmodulin binding" and "Cell junction" are highlighted. Confidence score cutoff: 0.4, only connected nodes are shown.

Materials

IMR90 clone 4 (WiCell #iPS(IMR90)-4)
Matrigel® Growth factor reduced (GFR) (Corning #356230)
mTESR1 medium (Stem Cell Technologies #85870)
Gentle cell dissociation reagent (Stem Cell Technologies #07174)
STEMdiff Dorsal Forebrain Organoid Differentiation Kit (Stem Cell Technologies #08620)
Aggrewell™800 24-well plates (Stem Cell Technologies #34815)
ROCK inhibitor, Y-27632 (Sigma-Aldrich, #SCM075)
Penicillin/Streptomycin (Gibco #15140)
Amphotericin B (Thermo Scientific #15290026)
H9 ESCs (WiCell, WA09)
StemFlex medium (Thermo Fisher Scientific, #A3349401)
Matrigel® (Corning, #356234)
STEMdiff Cerebral Organoid Kit (StemCell Technologies, #08570)
Ethylenediamine tetraacetic acid (Merck, #1.08418.1000)
Millicell Cell Culture Insert (Millipore, #PICMORG50)
Neurobasal (Thermo Fisher Scientific, #21103049)
B-27 supplement (Thermo Fisher Scientific, #17504044)
Glutamax (Thermo Fisher Scientific, #35050038),
Antibiotic-antimycotic (Thermo Fisher Scientific, #15240062)
Amphotericin B solution (Merck, #A2942-20ML)
D-(+)-Glucose (Sigma, #G7021)
Sucrose (Sigma, #84097)
Trizma base (Sigma #93352)
Dithiothreitol (DTT, Sigma #D9163)
Tissue grinder (15-ml Potter-Elvehjem type Teflon-glass tissue grinder, Wheaton, 358009)
Percoll™ solution (Cytiva, #17089102)
KCl (Sigma, #P9541)
NaCl (VWR, #27810.295)
HEPES (Sigma, #H3375)
$MgSO_4$ (Merck, # 7487-88-9)
$CaCl_2$ anhydrous (Merck, #2366663)
$Na_2HPO_4 \cdot 2H_2O$ (Merck, #1.06580.0500)
Sodium Pyruvate (Gibco, #11360)
$NaHCO_3$ anhydrous (Sigma, #71345)
10 kDa spin filters, Ultra-0.5 Centrifugal Filter Unit (Amicon, #UFC5010)
TEAB, Triethylammonium bicarbonate (Sigma #T7408)
Sodium deoxycholate (SDS, Sigma #D6750)
SafeSeal Microcentrifuge Tubes, Low-binding (Sorenson BioScience Inc.)
NanoPhotometer N60/N50 (Implen)
Iodoacetamide (Sigma #I1149)
Methylated trypsin (made in-house) [72]
LysC, Lysyl Endopeptidase (Wako, #129-02541)
Formic acid (Merck #1.11670.0250)
Pierce Quantitative Fluorometric Peptide Assay (Thermo, #23290)

Aurora Elite column 15 cm x 75 µm, C18 1.6 m (ESI Source Solutions)
Acetonitrile (VWR #83640.320)
TMTpro 16-plex (Thermo Fisher Scientific #A44520)
TMTpro 18-plex, TMTpro-134C & TMTpro-135N Label Reagents (Thermo Fisher Scientific #A52046)
Ammonium Formate (Riedel-de Haën #25204)
Trifluoroacetic acid (Merck #1.08178.0050)
Glycolic acid (Sigma #124737)
Ammonium hydroxide solution (Merck #1.05428.0500)
Titanium dioxide beads, 5 µm (GL Science #5020-75010)
Oasis HLB column (Waters #186000132)
Methanol (VWR #20864.320)
Reprosil-Pur 120 C18-AQ, 5 µm (Dr. Maisch GmbH, #r15.aq.)
Reprosil-Pur 120 C18-AQ, 3 µm (Dr. Maisch GmbH, # r13.aq.)
Acquity UPLC® -Class CSHTM C18 column (Waters)
Dionex Ultimate 3000 HPLC system (Thermo Fisher Scientific)
Formaldehyde Solution 16% w/v (Thermo Fisher Scientific #28908)
Phosphate buffered saline (Gibco #70011-036)
OCT Mounting media (VWR, #361603E)
Leica CM1860 cryostat (Leica Biosystems)
Superfrost® Plus Microscope slides (Thermo Fisher Scientific, #J1800AMNZ)
TritonX100 (Plusone #17-1315-01)
Donkey serum (BioWest, #S2170-100)
ProLong Diamond Antifade mountant (Invitrogen #P36965)
$NaH_2PO_4 \cdot H2O$ (Merck, #10049-21-5)
Batco agar (BD diagnostics, #214010)
Propylene oxide (Merck, #8070271000)
Epon (812 Resin, TAAB T031)
Glass knife (LKB Bromma 7800, Leica Microsystems)
Ultramicrotome (Reichert Ultracut S, Leica, Microsystems)
Toluidine blue (VWR, #34187.185)
Borex (VWR, #27727.231)
Diamond knife (MD1035)
150 mesh copper grids (Gilder, #G150-C3)
Parlodion-amyl acetate film (EMS)
Lead citrate (Reynold, #1963)
Bolt 4-12% Bis-Tris Plus Gels (Thermo Scientific #NW04125BOX)
NuPage LDS Sample buffer (Thermo Scientific # #NP0007)
NuPage Sample Reducing agent (Thermo Scientific, #NP0004)
PageRuler Plus pre-stained protein ladder (Thermo Scientific, #26620)
Trans-Blot® Turbo™ Transfer System (BioRad, #1704150)
PVDF membranes (Millipore, #IPVH08100)
TBS-Tween20 – TBS (Tris-base, NaCl, KCl (Sigma))-Tween20 (Sigma, #P1379)
Skim milk powder (VWR, #999999-99-4)
Anti-rabbit TOMM20 (Abcam, #ab186735)
Anti-rabbit Synapsin 1 (Abcam, #ab254349)
Mouse anti-Synaptophysin (Millipore, #S5768)

Anti-mouse β-actin HRP-linked (Abcam, #ab49900)
Anti-rabbit IgG, HRP-linked (Cell Signalling, #7074)
Anti-mouse IgG, HRP-linked (Abcam, #ab6728)
Immobilon ECL Ultra Western HRP Substrate (Millipore, #WBULS0100)
Amersham 680 Imager (GE Healthcare)